Red/NIR Thermally Activated Delayed Fluorescence from Aza-BODIPYs

Edurne Avellanal-Zaballa, Alejandro Prieto-Castañeda, Fernando García-Garrido, Antonia R. Agarrabeitia, María J. Ortiz, Esther Rebollar, Jorge Bañuelos and Inmaculada Garcia-Moreno**

E. Avellanal Zaballa, Dr. J. Bañuelos
Dpto. Química Física, Universidad del País Vasco (UPV/EHU), Aptdo. 644, 48080 Bilbao, Spain
E-mail: jorge.banuelos@ehu.es (JB)
A. Prieto-Castañeda, F. García-Garrido, Prof. A. R. Agarrabeitia, Prof. M. J. Ortiz.
Dpto. Química Orgánica, Universidad Complutense, Ciudad Universitaria s/n, 28006 Madrid, Spain
Dr. E. Rebollar, Prof. I. García-Moreno
Instituto Química-Física "Rocasolano", *IQFR-CSIC*, Serrano 119, 28006 Madrid, Spain
E-mail: i.garcia-moreno@iqfr.csic.es (IGM)

Keywords: delayed fluorescence, Aza-BODIPY, energy transfer, charge transfer, NIR emission, dye chemistry

The search for long-lived red and NIR fluorescent dyes is challenging and hitherto scarcely reported. Herein, the viability of aza-BODIPY skeleton as a promising system for achieving thermal activated delayed fluorescent probes (TADF) emitting in this target region is demonstrated for the first time. The synthetic versatile of this scaffold allows the design of energy and charge transfer cassettes modulating the stereoelectronic properties of the energy donors, the spacer moieties and the linkage positions. Delayed emission from these architectures is recorded in the red spectral region (695-735 nm) with lifetimes longer than 100 μs in aerated solutions at room temperature. The computational-aided photophysical study under mild and hard irradiation regimes disclose the interplay between molecular structure and photonic performance to develop long-lived fluorescence red emitters through thermally activated reverse intersystem crossing. The efficient and long-lasting NIR emission of the newly synthesized aza-BODIPY systems provides a basis to develop advanced optical materials with exciting and appealing photonic response.

1. Introduction

Over the last few years, an intense research effort has been focused on the design and synthesis of thermally activated delayed fluorescence (TADF) materials[1-5] liable of converting the excited T_1 states to emissive S_1 states by absorbing environmental thermal energy through an efficient reverse intersystem crossing (RISC).[6] Although a wealth of highly efficient blue[7-9] green,[10-12], yellow,[13,14] and orange[15,16] TADF emitters are presently available, the progress on achieving long-lived fluorophores emitting in the deep red part of the visible spectrum has unfortunately been slowed because it requires the optimization of contrasting properties.[17-20] The improved understanding of the processes governing the effectiveness of RISC process has already revealed some basic design principles on developing highly-effective red TADF emitters. [21-24] In this regard, the most effective strategy entails the synthesis of dyads with strong, rigid, chemically stable and sterically hindered donor and acceptor moieties spaced apart and twisted from each other through π-linker units.[25-31] These integrated molecular platforms fulfil the photophysical and electronic key requirements to enhance TADF process, such as: 1) low singlet-triplet energy gap; 2) an electronic coupling between donor and acceptor neither too strong nor too weak to enable both forward and reverse ISC processes;[28] 3) a large fluorescence rate constant; and 4) a high chemical, photochemical, and photophysical stability of the molecular building blocks.

Among the chemical structures tested to design red TADF probes, long-wavelength emitting aza-BODIPY fluorophores has never being considered for this application despite dyes based on this aza-BODIPY scaffold stand out as bright, stable, and compact red/NIR emitters.[32-34] In fact, the simple replacement of the *meso*-methine group at the BODIPY core by an electronegative nitrogen atom induces a pronounced bathochromic shift of both the absorption and emission transitions as well as a drastic decrease of the energy gap between

excited singlet and triplet states without promoting phosphorescence emission.[35] These effects can be enlarged through the peripherical arylation of the aza-BODIPY chromophoric core.[32-34] Recently, efficient and long-lasting fluorescent and laser emission in the target red/NIR spectral region have been recorded from polyarylated aza-BODIPYs under drastic pumping conditions.[36]

In this work, we report for the first time to the best of our knowledge red/NIR TADF emitters based on heavy-atom-free aza-BODIPY derivatives. The new dyes (**1-4**) were built up as highly-effective energy and charge transfer cassettes based on a BODIPY moiety acting as donor and covalently linked to a polyarylated-aza-BODIPY group acting as acceptor and red/NIR emitting unit (**Figure 1**). The chemical versatility of this chromophoric core allowed synthesizing a library of structurally related dyads by: 1) increasing the number of donor BODIPY units to intensify the energy and charge transfer efficiency; 2) tethering the donor units at the dipyrrin backbone as well as at the boron bridge of the acceptor unit; 3) modulating the link length between the donor-acceptor units through one or two phenyl rings acting as π-bridge ensuring no resonant interactions between the electronic clouds of the chromophoric subunits (via imposed steric hindrance and/or using the non-conjugated boron bridge as linkage position); and 4) enhancing the photoinduced electron transfer (PET) capability of the donor unit as a new approach to increase intersystem crossing without relying on the phosphorescence emission. [37] This synthetic strategy has yielded the first BODIPY-aza-BODIPY architectures displaying red/NIR delayed emission even in aerated solutions at room temperature despite thermal activated delayed fluorescence was easily quenching by oxygen, reducing drastically its effectiveness, which becomes one of the major challenges for the applicability of TADF probes.[38,39] A comprehensive analysis, aided by computational simulations, of the photonic signatures of these new red-emitting materials under soft- and drastic pumping conditions promoted an enhanced knowledge of the influence of the connecting modes between donor and acceptor units as well as of the underlying energy

and charge transfer processes over the effectiveness of RISC mechanism. In this regard, the present work arises as the first proof-of-concept elucidating the interplay of molecular design, structural factors and photonic behavior in red-emitting cassettes to boost aza-BODIPY scaffold as a smart chromophoric platform in developing advanced red/NIR TADF materials.

2. Results and Discussion

2.1. Synthesis and Chemical Characterization

Cassettes **1**, **2a** and **2b** were successfully obtained through Suzuki Miyaura reactions from the halogenated aza-BODIPY **5**[40] and the corresponding pinacol boronate BODIPY **6**[41] and **7**,[42] respectively (**Scheme 1A**). First, a mixture of the brominated aza-BODIPY **5** and pinacol boronate BODIPY **6** in presence of Na_2CO_3 as base and $Pd(PPh_3)_4$ as catalyst in a H_2O/THF/ toluene mixture were heated at 80 ºC under argon atmosphere for 10 h, affording the cassette **1**, in 26% yield. Similarly, cassette **2a** was isolated, in 77% yield, by reaction of **5** with **7**, under the same conditions, for 20 h. Finally, cassette **2b** (40%) was obtained also from **5** and **7** but using K_2CO_3 as base and carrying out the reaction under microwave irradiation at 120 ºC for 1 h.

Subsequently, cassettes **3**, **4a** and **4b** were synthesized by replacement of one or two fluorine atoms at the boron bridge of the aza-BODIPY **8**[43,44] by reaction with the corresponding 8-(4-hydroxyphenyl)BODIPY **9**[45] or **10**[46] in the presence of $AlCl_3$ as Lewis acid, according to the experimental procedure described in the literature[47] (**Scheme 1B**). All compounds were characterized using a combination of ^{1}H NMR, ^{13}C NMR, FTIR spectroscopy and high resolution mass spectrometry (HRMS). The synthesis and characterization of the new dyes are described in detail in Supporting Information.

2.2. Photophysical Properties. Energy Transfer *vs* Electron Transfer

The absorption spectra of the new cassettes feature two strong and clearly distinguishable bands in the visible spectral region (**Figures 2** and S1 in Supporting Information): the long

wavelength absorption owed to the π-extended aza-BODIPY through the peripheral aryl groups linked at its dipyrrin core (approaching 680 nm from the most arylated cassettes, **2a** and **2b**), whereas the short wavelength band was assigned to the pendant BODIPY moiety. In fact, the intensity of this last absorption band increased proportionally with the number of BODIPY subunits (**2a** *vs* **2b** in **Figure 2** or **4a** *vs* **4b** in **Figure S1** in Supporting Information) and its spectral position was bathochromically shifted by increasing the alkylation degree at the dipyrrin core of the BODIPY donor (**1** *vs* **2b**, **Figure 2** or **3** *vs* **4a** in **Figure S1** in Supporting Information). Therefore, the broadband absorption exhibited by the new cassettes resulted from the additive contribution of the transitions of each chromophoric subunit, being each one electronically decoupled as supported by the computed molecular orbitals (**Figures 3** and S2 in Supporting Information). Indeed, the molecular orbitals (MOs) involved in each electronic transition were just located at the polyarylated aza-BODIPY moiety or alternatively at the BODIPY units. On the other hand, the fluorescence spectra of the new cassettes were dominated by a long-wavelength emission (peaked up to 720 nm in **2b**) regardless of the excited absorption band, as consequence of an efficient intramolecular excitation energy transfer (EET) from the BODIPY donor to the energy acceptor and NIR emitting aza-BODIPY unit (**Figure 2** and S1 in Supporting Information). Actually, the emission from the donor BODIPY was almost negligible, yielding an EET efficiency close to the 100%, as it was expected owing to the short donor-acceptor distance and geometrical disposition imposed by their mutual covalent linkage.

However, the fluorescence efficiency showed a marked dependence on the alkylation degree of the BODIPY acting as energy donor; the cassettes bearing alkylated BODIPYs (tetramethylated in **3** or with further diethylation in **1**) became almost non-fluorescent (**Table** 1 and Table S1 in the Supporting Information). Quantum chemical calculations of the electronic density distribution based on DFT atomistic simulations (B3LYP/6-31G*) predicted that the alkylated BODIPY, grafted at both the boron atom as well as the dipyrrin

core of the aza-BODIPY, was able to act as energy donor but also as effective electron donor. Indeed, the HOMO state of these cassettes was entirely located on the BODIPY unit and energetically placed above the HOMO-1 and therefore within the energy gap responsible of the aza-BODIPY transition (Figure 3 and S2 in Supporting Information). Such energetic distribution of molecular orbitals (MOs) envisaged the ability of the alkylated BODIPY to effectively induce a reductive PET process upon excitation.[48] Thus, upon the photoinduced promotion of an electron from the HOMO to the LUMO+1 (under green excitation) or from HOMO-1 to LUMO (under red excitation), an electron transfer from the HOMO to the low-lying HOMO-1 was thermodynamically feasible. Such a reductive PET from the alkylated BODIPY grafted to the aza-BODIPY avoided radiative deactivation from LUMO back to the HOMO-1, thus explaining the almost negligible fluorescence emission recorded from **1** and **3**. Nevertheless, such undesirable PET pathway was totally suppressed just selecting fully non-alkylated BODIPY as energy donor units (**2a** and **2b**, or **4a** and **4b**). This substitution pattern lowered the energy of this HOMO state (i.e. from -5.32 eV in **3** to -5.77 eV in **4a**) to become HOMO-1 in these cassettes, being placed below the energy gap responsible of the aza-BODIPY electronic transitions (**Figures 3 and S2** in Supporting Information). This energetic rearrangement of the MOs hampered an effective PET process and, consequently, the fluorescence from the aza-BODIPY was restored, together with a substantial lengthening of the lifetime (**Table 1 and Table S1** in the Supporting Information).[49,50] This result denoted that the BODIPY functionalization was mainly involved in the composition of the HOMO state of these cassettes controlling the effectiveness of its final emission. Theodore software was used to account for the probability upon excitation of the charge transfer underlying the PET process[51] (scaled from 0 to 1). The cassettes **2b** and **4b** bearing non-alkylated BODIPY as energy donor sustained a very low charge transfer probability (just 0.10 and 0.02 respectively). However, the sole alkylation of the BODIPY (structural-related **1** and **3**, respectively) drastically increased the probability of transferring an electron from the

BODIPY subunit to the aza-BODIPY core (up to 0.78 and 0.72, respectively, in Table 1), supporting the viability of PET as the main non-radiative deactivation channel of the excited state in the cassettes featuring alkylated BODIPY as energy donors.

To support the viability of the predicted PET after anchoring alkylated energy donors to the aza-BODIPY, we conducted electrochemical measurements for the structural related pairs **1** vs. **2b**, and **3** vs. **4a** (**Figure S3** in the Supporting Information). Whereas no changes were detected in the cathodic region with the first reduction potential peaked at the same potential (-0.27 V), as expected in view of the almost invariant LUMO energy (**Figure 3** and **Figure S2** in the Supporting Information), the anodic region showed variations upon alkylation of the energy donor. Thus, the alkylation of the energy donor BODIPY decreased the oxidation potential of the corresponding aza-BODIPY cassettes (1.1 V for 1 and 1.2 V for **3**, vs. 1.3 V for **2b** and 1.4 V for **4a**, respectively). Such difference of 0.2 eV nicely correlates with the predicted decrease of the HOMO energy in these cassettes upon removal of the alkyls in the BODIPY acting as energy donors (**Figure 3** and **Figure S2** in the Supporting Information). Therefore, it is again confirmed that the BODIPY alkylation enables a thermodynamically driven PET.

It is noteworthy that the fluorescence enhancement upon removing the alkyl groups of the BODIPY energy donor depended also on its grafted position at the aza-BODIPY core (**Table 1** and **Table S1** in Supporting Information). Thus, the linkage through the 3,5-biphenyl groups (**2a** or **2b**) led to bright NIR emission (up to 30% with a lifetime of 2.3 ns) but this efficiency was greatly reduced (8% with a lifetime of just 1 ns) by linking the donor unit at the boron bridge of the aza-BODIPY (**4a** and **4b**). This markedly different behavior could be attributed to the conformational freedom of each unit inside the cassette, which should be less restricted in the systems based on boron functionalization. With respect to **2b**, the feasible rotation of the BODIPY units linked at the boron bridge in **4b** increased the

internal conversion deactivation process reducing consequently its fluorescence efficiency from 0.30 to a merely 0.08.

Therefore, cassette **2b**, which molecular design avoided deleterious effects (PET and internal conversion) on the emission quantum yield, stands out as NIR-emitter owing to both its more extended delocalized π-system and its high fluorescence efficiency, which became even 2-fold higher than that recorded from its isolated aza-BODIPY precursor **8** (**Table 1**).[36]

2.3. Photonic Behaviour Under Hard Pumping. Laser and Delayed Fluorescence

With the exception of the multichromophoric systems (**1** and **3**) sustaining a PET process, the photophysical behavior of the new BODIPY-aza-BODIPYs dyes as effective EET and ICT cassettes allowed them to lase efficiently in the red spectral region when they were transversally pumped at both 532 nm and 355 nm (second and third harmonic of a Nd:YAG laser, respectively). In fact, BODIPY-aza-BODIPY hybridation led to a drastic increase of the absorption at both pump lasing wavelengths with respect to that exhibited by the related monomeric aza-BODIPY **8.** This is a key factor from the point of view of the laser action, since it allowed reducing significantly the required gain-media concentrations avoiding, consequently, dye-solubility problems, emission quenching and/or aggregation processes, all of them with detrimental effects on laser action. Under the selected experimental conditions (transversal excitation and hard focusing of the incoming pumping radiation) the concentration in ethyl acetate which optimized the laser efficiency, understood as the ratio of the output and input energies, depended on the given dye and were ranging from 0.2 mM to 0.9 mM. The lasing properties of the new systems recorded under the mentioned experimental conditions are reported in **Table 2**. The BODIPY-aza-BODIPY systems exhibited lasing emission peaked in the red-edge of the visible spectrum, from 696 nm (**4a**) to 730 nm (**2b**) (**Table 2** and **Figure 4**). The dependence of the laser wavelength on the chemical structure of

the cassettes showed good correlation with the photophysical properties: the longer the fluorescence wavelength, the "redder" became the lasing emission.

Despite its low fluorescence quantum yield, the new dyes showed an unexpected high laser efficiency (up to 25 %), which was even higher than that exhibited by the monomeric aza-BODIPY **8** pumped at its maximum absorption wavelength.[36] This apparent mismatch can be rationalized taking into account the EET and ICT character of the emitting states in these cassettes leading to: a) a high Stokes shift (up to 700 cm^{-1}), which reduced the extension of re-absorption/re-emission processes and, thus, their deleterious effect in the laser action; b) a very short lifetime (below 0.6 ns), which ameliorated the population inversion and enhanced the stimulated emission probability, counterbalancing the low probability of spontaneous emission, and c) a high dipole moment (four- and six-fold higher than the isolated donor and acceptor fragments, respectively), allowing the molecular alignment with respect to the polarization of the exciting laser beam to enhance the emission efficiency of the media.[52] In this regard, the chemical modification around the boron atom had low impact in the laser efficiency of the corresponding derivatives (**4a** and **4b**) since the recorded decrease of the fluorescence efficiency upon replacement of the fluorine atom also entailed a drastic shortening of the corresponding lifetime (**Table 1**).

In terms of traceability and feasibility of red photonic materials, efficiency is not the only crucial variable to be considered. A further important parameter is the photostability of the emission over long operation times. Ideally, a high resistance to active medium photodegradation under repeated pumping is sought after. A reasonable evaluation of the photostability of laser materials can be obtained by irradiating a small amount of solution with exactly the same pumping energy and geometry as used in the laser experiments, and monitoring the evaluation of the laser-induced fluorescence (LIF) intensity with respect to the number of pump pulses (see Supporting Information). This experimental set-up allowed us to analyze even the long-term photostability of the cassettes **1** and **3** since the PET process

induced by its molecular structure was able to turn the laser action off but did not extinguish LIF emission. To proper compare the intrinsic photodegradation rate of the active media irrespective of the cavity configuration/parameters and sample concentrations used, we introduced a normalized photostability parameter such as the accumulated pump energy absorbed by the system, per mole of dye, before the output energy falls to a 10% of its initial value (E_{dose} in GJ·mol^{-1}). As it was expected, the new cassettes based on robust building blocks exhibited good photostability since up to 160 GJ·mol^{-1} were required for inducing a 10% decrease of its LIF emission (**Table 2**). Energy transfer from the peripheral BODIPYs to the central red-emitting aza-BODIPY reduced the rate and extension of the photodegradation processes and significantly enhanced the photostability of the multichromophoric systems with respect to the own monomeric aza-BODIPY **8**, as well as other monomeric commercial laser dyes with emission in the same spectral region.[36] This enhanced photostability was widespread to all the cassettes herein developed regardless of the acting EET, ICT and even PET mechanism sustained by its molecular design. Actually, the lasing action attending to both lasing efficiency and photostability depended on the number of donor units joined to the aza-BODIPY framework more than on its linkage length and/or position: the highest the number of peripheral BODIPYs acting as donor units the highest became the lasing efficiency and photostability (**Table 2**).

Other additional advantage of the light-harvesting molecular design of these cassettes is the excitation versatility allowing to be efficient pumped also in the UV region of the visible spectrum. In fact, upon laser photoexcitation at 355 nm, the newly synthetized cassettes displayed a lasing behavior (attending to lasing wavelength, efficiency and photostability) similar to those recorded pumping at 532 nm (**Table 2**). Further enhancement of the photonic behavior on going from the monomeric dye **8** to the multichromophoric cassettes was recorded pumping **8** at 532 nm and 355 nm instead of at its maximum absorption wavelength.[36] To overcome the low absorption of **8** at these laser pump

wavelengths highly concentrated solutions (up to 5-fold higher than those required for the cassettes) were needed. As it was mentioned above, this experimental issue had a deleterious effect on the laser action and, consequently, a 3-fold decrease in the lasing efficiency and photostability of **8** were recorded with respect to the values achieved pumping it at 654 nm.[36]

To get more inside on the photonic behavior of the newly synthesized aza-BODIPY cassettes time-gated emission related to its monomeric parent dye **8** was further investigated by irradiating the samples within the same optical configuration used in the laser characterization but under experimental conditions, attending to both dye concentration and pump laser fluence, well below the threshold for onset the laser action. To meet this requirement the analysis was carried out for dye concentrations and energy fluences lower than 0.2 mM and 32 mJ/cm^2, respectively. Time-gated emission induced by laser pulses at 532 and 355 nm was detected with an intensified camera (iStar, Andor Technologies) coupled to a spectrograph (Kymera 193i-A, Andor Technologies). The camera enabled gate widths ranging from nanoseconds up to seconds and its opening can be delayed in a control way with respect to the incoming pump laser. It should be noted that neither long-pass-filters nor band-pass filters were used to remove the excitation laser since we verified that these filters (especially long pass filters) under drastic pump conditions exhibited its own fluorescence and/or phosphorescence emission, which could lead to misunderstanding the experimental results. This experimental set-up allowed to carry out the measurements even under adverse conditions, such as aerated solutions and at room temperature, in which the emission efficiency could become critically quenched.

Following exposure to intense laser pulses at both 355 nm and 532 nm all the new synthesized cassettes as well as the monomeric parent **8** exhibited delayed emission able to be registered at delay times longer than 100 μs with respect to the incoming laser pump radiation (**Figures 5** and **S4** in Supporting Information). Delayed emission appeared with similar spectral profile that the prompt laser-induced fluorescence and it did not change over time-

exposure except for a steady decrease of its intensity as the delay time was increased (**Figure 5**). This is the first time to the best of our knowledge that delayed emission was recorded from fluorophores based on aza-BODIPY scaffold, including both monomeric dyes and homo- and hetero-multichromophoric systems, although our experimental arrangement did not allow determining properly the efficiency of this delayed emission. Considering that the prompt fluorescence had lifetimes as short as 2 ns, delayed emission with lifetimes longer than 100 μs must unequivocally imply long-lived triplet excited states. In this regard, it should be noted that neither solvents (i.e. iodoethane) nor triplet sensitizers were added to the dye solution trying to enhance the triplet quantum yield since at the same time the external heavy atom shortened the triplet lifetime. Two mechanisms can induce this delayed emission: thermally activated delayed fluorescence (TADF) or triplet-triplet annihilation (TTA). To distinguish between these two different processes the influence of different experimental and structural parameters on the delayed emission was systematically analyzed.

1.- Small singlet-triplet energy gap is required to facilitate the RISC process in TADF probes. It is well known that the ISC probability in BODIPYs is extremely low (just a 1% of the excited electrons populate triplet excited states).[53,54] Advanced excited state calculations for the simplest BODIPY core revealed that the most feasible ISC funnel along the deactivation of the S_1 state took place through the conical intersection with the high-lying T_2 state.[55] Interestingly, and according to this study, the origin of an ineffective ISC in BODIPYs was not only the energy barrier to access to the S_1-T_2 conical intersection (around 0.4-0.5 eV) but rather the very low spin-orbit coupling (1 cm^{-1}).

Trying to estimate the ISC probability in both the aza-BODIPY scaffold and the large-sized cassettes derived from it, we approached tentatively the S-T energy gap via Franck-Condon transitions (**Figure S5** in Supporting Information for details). In this regard, it should be noted that unlike the simplest BODIPY, the large molecular size of the herein synthesized cassettes hampered more advanced simulations and excited state calculations. In the

monomeric **8** aza-BODIPY as well as in the newly synthesized dyads the excited state S_1 and the closest triplet state (T_2 in aza-BODIPYs or T_3 in their corresponding cassettes) were almost energetically degenerate (energy gap < 20 meV). In this energetic picture, upon strong pumping, an electron in the excited state could reach the conical intersection to access a high-lying triplet state. However, once there, instead of relaxing down to the triplet states by internal conversion, it could come back to the S_1 state via a thermodinamically feasible RISC allowing to record delayed fluorescence in a time-scale of hundreds of microseconds.

2.- Strengthening the donor character of the final molecule on going from one donor to two donor units linked to the aza-BODIPY moiety (for instead **2a** and **2b**), some photophysical parameters critical for the effectiveness of TADF emission became enhanced. In fact, matching the optical density of **2a** and **2b** at the excitation wavelength (532 nm), an emission at delay time higher than 150 μs could be recorded from **2b,** while **2a** with only a donor BODIPY unit showed considerable less and shorter delayed fluorescence since no emission was registered beyond 100 μs.

3.- The replacement of the *meso*-methine group in the BODIPY core by an electronegative aza-N atom induced a marked change in the internal electronic properties due to the delocalization of the N electron lone pair along the dipyrrin framework. Since the *meso* position greatly contributed to the LUMO state upon excitation,[36] the electronic transitions in the new dyads gained n-π* character compared to the BODIPYs, which could enhance the spin-orbit coupling and the ensuing ISC.[56] In fact, according to the El-Sayed rule, the low-lying nπ*states significantly speed up the RISC transition compared to the TADF emitters where only ππ*excitons are energetically accessible.[57,58] Thus, as theoretically supported (**Figure S5** in Supporting Information), the qualitatively approached singlet-triplet energy gap should decrease but without promoting the triplet emission in aza-BODIPY.[35] As a result, either in the monomeric **8** aza-BODIPY or in the new **1-4** dyads we were unable to detect

neither the phosphorescence emission nor the singlet oxygen emission sensitized from the corresponding triplet states.

4.- Since the triplet concentration can be varied by dilution and/or by modulating the pump laser energy, the intensity of the emission delayed 10 μs was recorded decreasing the dye concentration or the laser fluence. Under these experimental conditions the intensity of the delayed emission decreased linearly following therefore the expected dependence in one-photon process (**Figures S6** and **S7** in Supporting Information.). Furthermore, we never observed the quadratic dependence of the emission intensity on dye concentration and/or laser power required in a two-photon process such as triplet-triplet annihilation.

These results indicated that the delayed emission of the monomeric aza-BODIPY **8** and the herein synthesized multichromophoric cassettes should decay from the singlet excited state populated through RISC from the corresponding long-lived triplet excited states with no contribution of any other processes such as TTA. Hence the aza-BODIPY moiety became an effective TADF probe maintaining a long-lived fluorescence emission in the red/near IR spectral region to boost its applicability in strategic research fields.

3. Conclusion

Red/NIR thermally activated delayed fluorescence from dyes based on aza-BODIPY scaffolds was reported for the first time to the best of our knowledge. Thermally activated delayed fluorescence emission from 680 to 800 nm was registered even in aerated solutions at room temperature upon laser excitation at both 532 and 355 nm. Aza-BODIPYs due to the replacement of the central *meso*-carbon by an electronegative aza group became a better electron acceptor than the own BODIPY, thus being prone to electron transfer processes. A new series of cassettes based on grafting aza-BODIPY, acting as acceptor and red-emitting moiety, with one or two BODIPY donor units allowed to achieve a subtle balance between

competing exciton energy and charge transfer processes to modulate properly the fluorescence response just adjusting the stereoelectronic properties of the energy donors, spacers and linkage positions.

The computational-assisted analysis of the photonic behaviour of the herein synthesized energy and charge transfer cassettes revealed some key structural guidelines to enhance their prompt and delayed emission signatures with respect to that achieved from its monomeric aza-BODIPY. The new cassettes showed efficient light-harvesting properties across the UV-visible spectral region owing to the imposed steric hindrance to avoid both resonant electronic interactions as well as supramolecular aggregation by π-π stacking interactions, with deleterious effects on the emission efficiency. Thus, a judicious election of the BODIPY energy donors was crucial to avoid PET and to enable bright emission. Such modulation of the electron releasing ability of the energy donors can be straightforwardly done just adjusting the alkylation degree of the electron donors. In fact, non-alkylated BODIPY allowed suppressing PET and achieving bright NIR emission regardless of the excitation wavelength. Thereby, upon laser excitation at both 355 and 532 nm, these cassettes lased beyond 700 nm, with efficiencies and photostabilities higher than those recorded from the monomeric aza-BODIPY as well as other commercially available dyes with emission in the red-edge of the visible spectrum and pumped under otherwise identical experimental conditions.

In addition, our synthetic approach fulfilled all the energetic and electronic requirements to achieve red/NIR emission delayed more than 100 μs with respect to the incoming radiation, regardless on the laser pumping wavelength as well as on the excitation transfer mechanism sustained by the molecular design. Through a systematic experimental and theoretical analysis of this surprising photonic behaviour we unambiguously identified thermally activated reverse intersystem crossing from long-lived triplet excited states as the mechanism responsible for the observed delayed emission with no contribution of any other

processes such could be triplet-triplet annihilation. These outstanding results pointed out the rational design of BODIPY-aza-BODIPY cassettes as a promising starting point from developing novel long-lived TADF materials with emission in the strategic red/NIR spectral region boosting their medical and optoelectronic applications.

Acknowledgements
We gratefully acknowledge the Spanish *Ministerio de Economia y Competitividad* for financial support (projects MAT2017-83856-C3-1-P, 2-P and 3-P). We also thank the *Gobierno Vasco* for financial support (project IT912-16) and for a predoctoral fellowship to E. A.-Z. The authors thank SGIker of UPV/EHU for technical support with the computational calculations, which were carried out in the "arina" informatic cluster.

References

[1] T. Li, D. Yang, L. Zhai, S. Wang, B. Zhao, N. Fu, L. Wang, Y. Tao, W. Huang, *Adv. Sci*. **2017**, *4*, 1600166.

[2] Z. Yang, Z. Mao, Z. Xie, Y. Zhang, S. Liu, J. Zhao, J. Xu, Z. Chi, M. P. Aldred, *Chem. Soc. Rev*. **2017**, *46*, 915-1016.

[3] X.-K. Chen, D. Kim, J.-L. Brédas, *Acc. Chem. Res.* **2018**, *51,* 2215-2224.

[4] Y. Liu, Ch. Li, Z. Ren, S. Yan, M. R. Bryce, *Nat. Rev. Mater*. **2018**, 18020

[5] X. Liang, Z.-L. Tu, Y.-X. Zheng, *Chem. Eur. J.* **2019**, *25*, 5623-5642.

[6] C. Baleizao, M. N. Berberan-Santos, *J. Chem. Phys.* **2007**, *126*, 204510.

[7] Q. Zhang, B. Li, S. Huang, H. Nomura, H. Tanaka, C. Adachi, *Nat. Photonics*, **2014**, *8*, 326-332.

[8] S.-J. Woo, Y. Kim, M.-J. Kim, J. Y. Baek, S.-K. Know, Y.-H. Kim, J.-J. Kim, *Chem. Mater*. **2018**, *30,* 857-863.

[9] C.-S. Oh, D. Sa Pereira, S. H. Han, H-J. Park, H. F. Higginbotham, A. P. Monkmman, J. Y. Lee, *ACS Appl. Mater. Interfaces* **2018,** *10*, 35420-35429.

[10] C. W. Lee, J. Y. Lee, *ACS Appl. Mater. Interfaces* **2015**, *7*, 2899-2904.

[11] D. R. Lee, B. S. Kim, C. W. Lee, Y. Im, K. S. Yook, S.-H. Hwang, J. Y. Lee, *ACS Appl. Mater. Interfaces*, **2015**, *7*, 9625-9629.

[12] C. Deng, S. Zheng, D. Wang, J. Yang, Y. Yue, M. Li, Y. Zhou, S. Niu, L. Tao, T. Tsuboi, Q. Zhang, *J. Phys. Chem. C.* **2019**, *49,* 29875-29883.

[13] X.-L. Li, G. Xie, M. Liu, D. Chen, X. Cai, J. Peng, Y. Cao, S.-J. Su, *Adv. Mater* .**2016**, *28*, 4614-4619.

[14] D. Chen, P. Rajamalli, F. Tenopala-Carmona, C. L. Carpenter-Warren, D. B. Cordes, C.-M. Keum, A. M. Z. Slawin, M. C. Gather, E. Zysman-Colman, *Adv. Opt. Mater*. **2020**, *8*, 1901283.

[15] W. Zeng, H.-Y. Lai, W.-K. Lee, M. Jiao, Y.-J. Shiu, C. Zhong, S. Gong, T. Zhou, G. Xie, M. Sarma, K.-T. Wong, C.-C. Wu, C. Yang, *Adv. Mater.* **2018**, *30*, 1704961.

[16] J.-X. Chen, W.-W. Tao, Y.-F. Xiao, K. Wang, M.Zhang, X.-Ch. Fan, W.-C. Chen, J. Yu, S. Li, F.-X. Geng, X.-H. Zhang, C.-S. Lee, *ACS Appl. Mater. Interfaces*, **2019**, *32*, 29086-29093.

[17] S. Wang, Z. Cheng, X. Song, X. Yan, K. Ye, Y. Lu, G. Yang, Y. Wang, *ACS Appl. Mater. Interfaces*, **2017**, *9*, 9892-9901.

[18] J. H. Kim, J. H. Yun, J. Y. Lee, *Adv. Optical Mater.* **2018**, *6*, 1800255.

[19] J.-X. Chen, W.-W. Tao, W.-C. Chen, Y.-F. Xiao, K. Wang, C. Cao, J. Yu, S. Li, F.-X. Geng, C. Adachi, C.-S. Lee, X.-H. Zhang, *Angew. Chem. Int. Ed*. **2019**, *58*, 14660-14665.

[20] X. Gong, P. Li, Y.-H. Huang, C.Y. Wang, C. H. Lu, W.-K. Lee *Adv. Funct. Mater*. **2020,** 1908839.

[21] M. K. Etherington, J. Gibson, H. F. Higginbotham, T. J. Penfold, A. P. Monkman *Nat. Commun.* **2016**, *7*, 13680.

[22] J. Gibson, T. J. Penfold, *PhysChemChemPhys*, **2017**, *19*, 8428-8434.

[23] T. J. Penfold, F. B. Dias, P. Monkman, *Chem. Commun*. **2018**, *54,* 3926-3935.

[24] X. K. Chen, D. Kim, J. L. Bredas, *Acc. Chem. Res*. **2018**, *51*, 2215-2224.

[25] Y. Im, M. Kim, Y.-J. Cho, J.-A. Seo, K. S. Yook, J. Y. Lee, *Chem. Mater*. **2017**, 5, 1946-1963.

[26] Q. Zhang, H. Kuwabara, W. J. Potscavage, S. Huang, Y. Hatae, T. Shibata, C. Adachi, *J. Am. Chem. Soc*. **2014**, *136*, 18070-18081.

[27] G. A. Sommer, L. N. Mataranga-Popa, R. Czerwieniec, T. Hofbeck, H. H. H. Homeier, T.J.J. Müller, H. Yersin, *J. Phys. Chem. Lett*. **2018**, *13*, 3692-3697.

[28] G. Tang, A. A. Sukhanov, J. Zhao, W. Yang, Z. Wang, Q. Liu, V. K. Voronkova, M. Di Donato, D. Escudero, D. Jacquemin, *J. Phys. Chem. C*, **2019**, *123*, 30171-30186.

[29] F. Gao, R. Du, C. Han, J. Zhang, Y. Wei, G. Lu, H. Xu, *Chem. Sci*, **2019**, 10, 5556-5567.

[30] D. G. Congrave, B.H. Drummond, P. J. Conaghan, H. Francis, S. T .E. Jones, C. P. Grey, N. C. Greenham, D. Credgington, H. Bronstein, *J. Am. Chem. Soc*. **2019**, 141, 18390-18394.

[31] S. Izumi, H. F. Higginbotham, A. Nyga, P. Stachelek, N. Tohnai, P. de Silva, P. Data, Y. Takeda, S. Minakata, *J. Am. Chem. Soc*. **2020**, *142*, 1482-1491.

[32] Y. Ge, D. F. O´Shea, *Chem. Soc. Rev.* **2016**, *45*, 3846-3864.

[33] S. Kumar, K. G. Thorat, M. Ravikanth, *J. Org. Chem*. **2017**, *82*, 6568-6577.

[34] S. Shimizu, *Chem. Commun*. **2019**, *55*, 8722-8743.

[35] J. K. G. Karlsson, A. Harriman, *J. Phys. Chem. A*, **2016**, *120*, 2537-2546.

[36] A. Prieto-Castañeda, E. Avellanal-Zaballa, L. Garztia-Rivero, L. Cerdan, A. R. Agarrabeitia, I. García-Moreno, J. Bañuelos, M. J. Ortiz, *ChemPhotoChem,* **2019**, *3*, 75-85.

[37] M. A. Filatov, S. Karuthedath, P. M. Poletshuk, H. Savoie, K. J. Flanagan, C. Sy, E. Sitte, M. Telitchko, F. Laquai, R. W. Bpyle, M.O. Senge, *J. Am. Chem. Soc*. **2017**, *139*, 6282-6285.

[38] Q. Zhang, S. Xu, M. Li, Y. Wang, N. Zhang, Y. Guan, M. Chen, C.-F. Chen, H.-Y. Hu, *Chem. Commun.* **2019,** *55,* 5639-5642.

[39] Y. Wu, L. Jiao, F. Song, M. Chen, D. Liu, W. Yang, Y. Sun, G. Hong, L. Liu, X. Peng, *Chem.Commun*. **2019**, *55*, 14522-14525.

[40] P.-A. Bouit, K. Kamada, P. Feneyrou, G. Berginc, L. Toupet, O. Maury, C. Andraud, *Adv. Mater*. **2009**, *21*, 1151-1154.

[41] M. Koepf, M. Trabolsi, J. A. Wytko, D. Paul, A. M. Albrecht-Gary, J. Weiss, *Org. Lett.* **2005**, *7*, 1279-1282.

[42] Z. Liu, S. G. Thacker, S. Fernandez-Castillejo, E. B. Neufeld, A. T. Remaley, R. Bittman, *ChemBioChem* **2014**, *15*, 2087-2096.

[43] G. Sathyamoorthi, M.-L. Soong, T. W. Ross, J. H. Boyer, *Heteroat. Chem*. **1993**, *4*, 603-608.

[44] A. Gorman, J. Killoran, C. O´Shea, T. Kenna, W. M. Gallagher, D. F. O´Shea, *J. Am. Chem. Soc.* **2004**, *126*, 10619-10631.

[45] A. Coskun, E. Deniz, E. U. Akkaya, *Org. Lett*. **2005**, *7*, 5187-5189.

[46] D. Prasannan, D. Raghav, S. Sujatha, H. Hareendrakrishna Kumar, K. Rathinasamy, C. Arunkumar, *RSC Adv.* **2016**, *6*, 80808-80824.

[47] G. Durán-Sampedro, A. R. Agarrabeitia, L. Cerdán, M. E. Pérez-Ojeda, A. Costela, I. García-Moreno, I. Esnal, J. Bañuelos, I. López Arbeloa, M. J. Ortiz, *Adv. Funct. Mater.* **2013**, *23*, 4195-4205.

[48] M. E. El-Khouly, A.N. Amin, M. E. Zandler, S. Fukuzumi, F. D´Souza, *Chem. Eur. J* **2012,** *18*, 5239-5247.

[49] S. Kumar, H. B. Gobeze, T. Chatterjee, F. D´Souza, M. Ravikanth, *J. Phys Chem A* **2015**, *119*, 8338-8348.

[50] S. Kumar, K. G. Thorat, M. Ravikanth, *J. Org. Chem*. **2017**, *82*, 6568-6577.

[51] D. Escudero, *Acc. Chem. Res***. 2016**, *49*, 9, 1816-1824.

[52] L. Cerdan, A. Costela, I. Garcia-Moreno, J. Bañuelos, I. Lopez Arbeloa, *Laser Phys. Lett*. **2012**, *9*, 426-433.

[53] A. Schmitt, B. Hinkeldey, M. Wild, G. Jung, *J. Fluoresc*., **2009** *19*, 755-758.

[54] J. Zhao, K. Xu, W. Yang, Z. Wang, F. Zhong, *Chem. Soc. Rev*. **2015**, *44*, 8904-8939.

[55] M. de Vetta, L. Gonzalez, I. Corral, *ChemPhotoChem* **2019**, *3*, 727-738.

[56] R. T. Kuznetsova, Y. V. Aksenova, D. E. Bashkirtsev, A. A. Prokopenko, E. N. Tel´minov, G. V. Mayer, N. A. Dudina, E. V. Antina, A. Y. Nikonova, M. B. Berezin, A. S. Semeikin, *High Energy Chem*. **2015**, *49*, 16-23.

[57] F. B. Dias, K. N. Bourdakos, V. Jankus, K. C. Moss, K. T. Kamtekar, V. Bhalla, J. Santos, M. R. Bryce, A. P. Monkman, *Adv. Mater*., **2013**, *25,* 3707-3714.

[58] I. Lyskov, C. M. Marian, *J.Phys.Chem. C,* **2017**, *121*, 21145-21153.

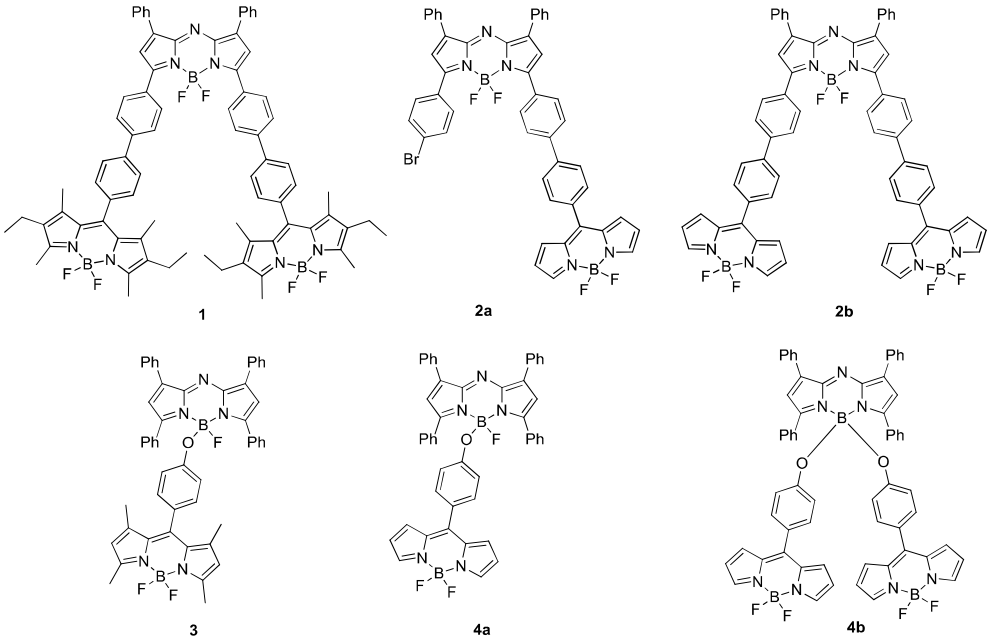

Figure 1. The structures of cassettes aza-BODIPY/BODIPY synthesized.

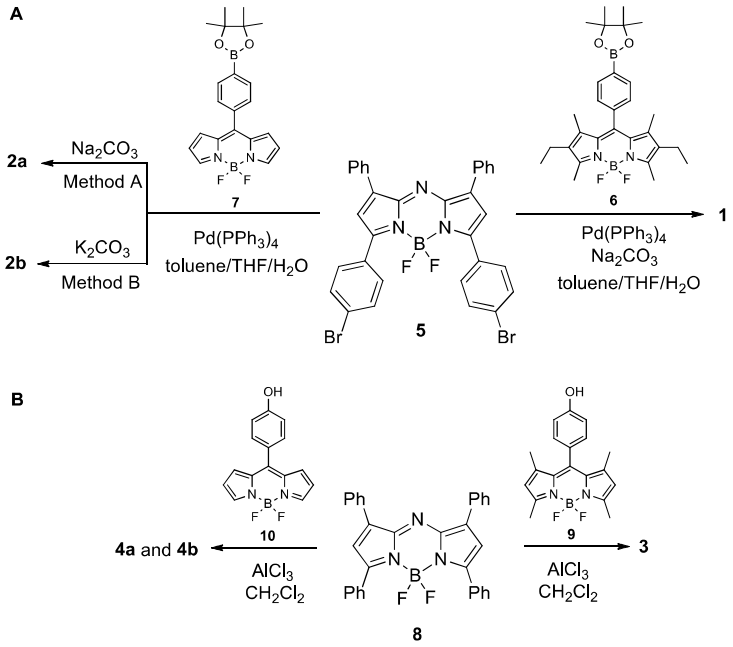

Scheme 1. Synthesis of cassettes aza-BODIPY/BODIPY **1-4**.

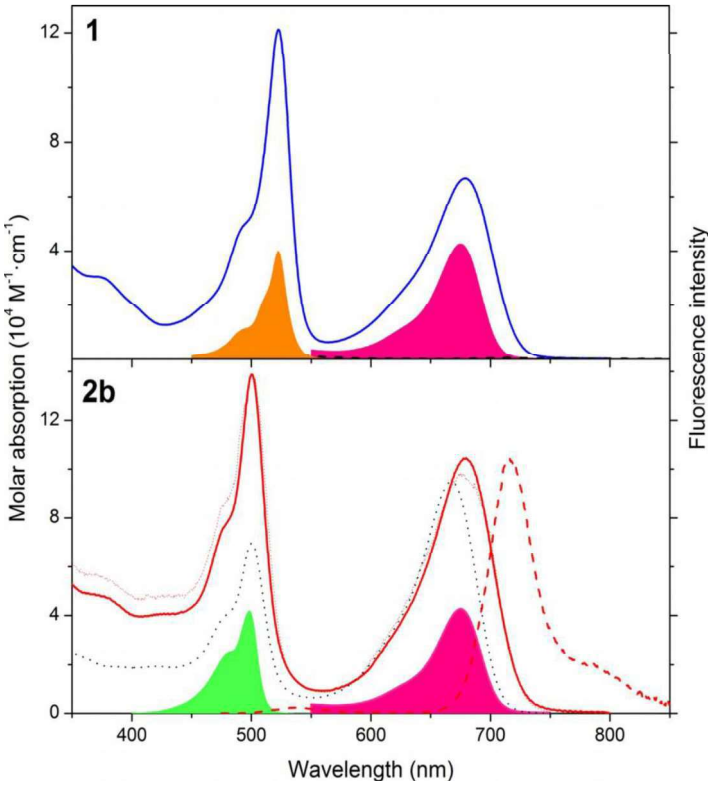

Figure 2. Absorption and fluorescence (dashed, after selective excitation of the BODIPY donor) and spectra of the triads linked through a biphenyl spacer (**1** and **2b**) in diluted solutions of ethyl acetate. The excitation spectrum (dotted, monitored at the aza-BODIPY emission) of **2b** is also included. To highlight the effect of the number of appended BODIPY donors, the absorption spectrum of the **2a** dyad is also included for comparison (dotted line in black). The absorption spectra (filled bands) of the isolated building blocks of the cassettes are also added to evidence the maintenance of the integrity of the chromophores after its covalent linkage. The corresponding spectra for the cassettes **3** and **4b**, linked at the boron atom, are collected in Figure S1 in Supporting Information.

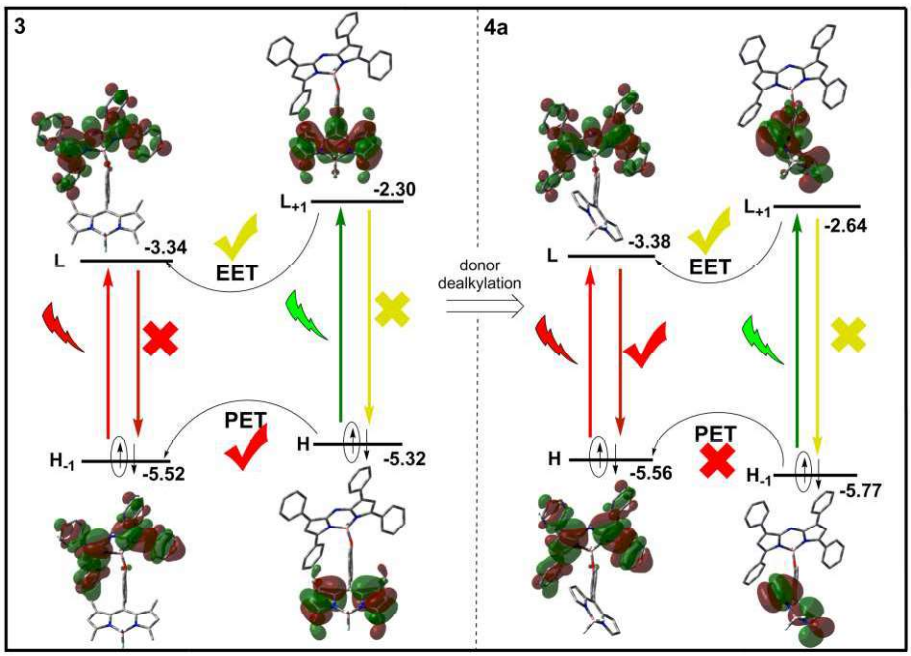

Figure 3. Computed molecular orbitals (b3lyp/6-31g*) and energies from the analogs **3** and **4a** differing just in the methylation of the energy donor BODIPY tethered at the boron of the

aza-BODIPY. The probability of the competing fluorescence, EET and PET processes is depicted. The corresponding MOs diagram for the cassettes **1** and **2b**, linked at the 3,5-biphenyl group of the aza-BODIPY core, are collected in Figure S2 in Supporting Information.

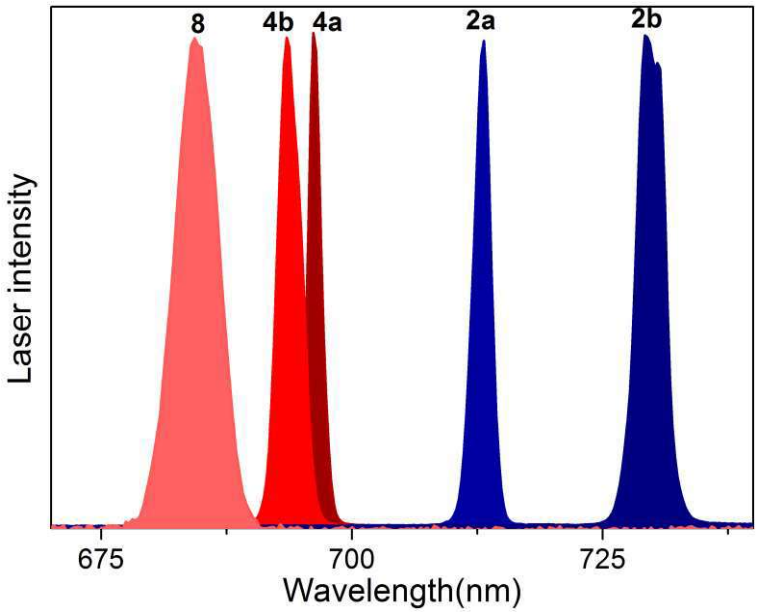

Figure 4. Normalized laser spectra of **2a**, **2b**, **4a** and **4b** in ethyl acetate solution at a concentration 0.5 mM pumped with laser pulses at 532 nm and 35 mJ/cm^2 fluence. The corresponding spectrum of its monomeric parent dye **8** was also included for comparison purposes.

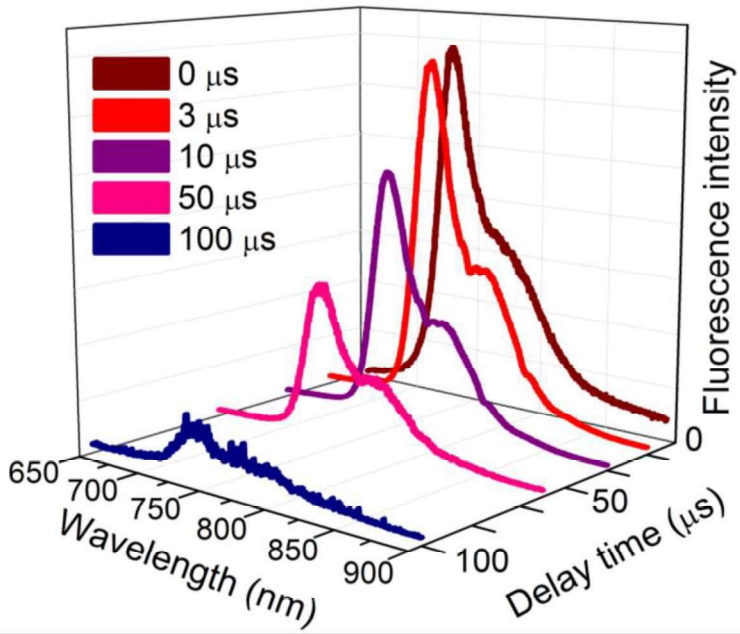

Figure 5. Delay time-dependent evolution of the fluorescence spectrum of **2b** in aerated ethyl acetate solution (0.1 mM) at room temperature upon excitation with laser pulses at 532 nm and 20 mJ/cm^2 fluence. The prompt laser-induced fluorescence spectrum recorded under otherwise identical experimental conditions is also included for comparison. Note that the prompt fluorescence has been normalized to the intensity of the 3 μs delayed emission in order to demonstrate full spectral coincidence. However, its non-normalized intensity corresponds to a factor ×3, which does not apply because rescaling the delayed emissions for times longer than 50 μs would hardly be appreciated.

Table 1. Photophysical properties of all the cassettes in diluted solutions (2 μM) of ethyl acetate. The corresponding data of the isolated energy acceptor aza-BODIPY **8** are added for comparison.[36] The corresponding data in nonpolar and polar media are collected in Table S1 in the Supporting Information.

	λ_{ab} (nm)	ε_{max} ($10^4 M^{-1}\cdot cm^{-1}$)	λ_{fl} (nm)	Φ	τ (ns)	k_{fl} (10^8 s^{-1})	k_{nr} (10^8 s^{-1})
1	678.5	6.7	711.5	0.006	NR	-	-
	523.0	12.1					
2a	667.5	7.7	701.0	0.24	1.83	1.31	4.15
	500.5	5.7					
2b	680.0	10.4	718.5	0.30	2.28	1.31	3.07
	500.5	13.9					
3	651.5	3.9	672.5	0.007	NR	-	-
	497.5	5.3					
4a	649.5	8.2	675.0	0.08	0.84	0.95	10.9
	494.5	7.7					
4b	655.0	7.2	678.5	0.08	1.03	0.77	8.93
	494.5	13.3					
8	646.0	8.6	668.0	0.12	0.81	1.48	9.64

absorption wavelengths (λ_{ab}); molar extinction coefficients at the absorption maxima (ε_{max}); fluorescence wavelength (λ_{fl}); fluorescence quantum yield (ϕ); fluorescence lifetimes (τ, being independent of the excitation wavelength), radiative (k_{fl}) and non-radiative (k_{nr}) deactivation rate constants

NR: non-recorded because they are below 50ps, the time resolution of the photon counter.

Table 2. Lasing properties and photostability of the new synthesized aza-BODIPY cassettes in ethyl acetate solution at the concentration which optimizes the laser efficiency of each dye pumped at both wavelengths, 355 and 532 nm. The lasing behaviour of the monomeric dye **8** pumped under identical experimental conditions are also include for comparison purposes

	532 nm				355 nm			
Dye	[C] (mM)	%Eff	λ_{la} (nm)	E_{dose} (GJ/mol)	[C] (mM)	%Eff	λ_{la} (nm)	E_{dose} (GJ/mol
1			729[a]	160				
2a	0.9	22	712	76	0.5	19	709	62
2b	0.5	25	730	142	0.3	21	725	123
3			720[a]	81				
4a	0.8	21	696	64	0.4	15	694	
4b	0.9	23	693	145	0.4	16	690	135
8	2.0	6	689	22	1.6	4	685	

[a]laser induced fluorescence

Keyword charge transfer, delayed fluorescence, dye chemistry, energy transfer, NIR emission

Edurne Avellanal-Zaballa, Alejandro Prieto-Castañeda, Fernando García-Garrido, Antonia R. Agarrabeitia, María J. Ortiz, Ester Rebollar, Jorge Bañuelos* and Inmaculada Garcia-Moreno*

Red/NIR Thermally Activated Delayed Fluorescence from Aza-BODIPYs

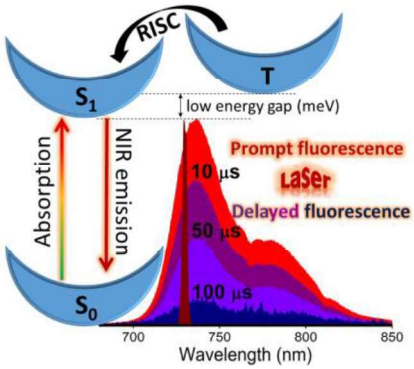

Supporting Information

Red/NIR Thermally Activated Delayed Fluorescence from Aza-BODIPYs

Edurne Avellanal-Zaballa, Alejandro Prieto-Castañeda, Fernando García-Garrido, Antonia R. Agarrabeitia, María J. Ortiz, Ester Rebollar, Jorge Bañuelos and Inmaculada Garcia-Moreno**

Table of content

1. General methods

Synthesis: All starting materials and reagents were commercial, unless otherwise indicated, and used without further purifications. Common solvents were dried and distilled by standard procedures. Flash chromatography was performed using silica gel (230-400 mesh). NMR spectra were recorded using $CDCl_3$ at 20 ºC. ^1H NMR and ^{13}C NMR chemical shifts (δ) were referenced to internal solvent $CDCl_3$ (δ = 7.260 and 77.03 ppm, respectively). DEPT 135 experiments were used to determine the type of carbon nucleus (C *vs* CH *vs* CH_2 vs. CH_3). FTIR spectra were obtained from neat samples using the ATR technique. Melting points were determined in open capillaries and are uncorrected. High resolution mass spectrometry (HRMS) were performed using the MALDI-TOF technique.

Photophysical properties: The photophysical properties were registered in diluted solutions (around 2×10^{-6} M), prepared by diluting a concentrated stock solution in ethyl acetate (spectroscopic grade). UV-Vis absorption and fluorescence spectra were recorded on a Varian model CARY 4E spectrophotometer and an Edinburgh Instruments spectrofluorimeter (model FLSP 920), respectively. Fluorescence quantum yields (ϕ) were obtained using a zinc phthalocyanine (ϕ = 0.30 in toluene with 1% of pyridine) as reference, from corrected spectra (detector sensibility to the wavelength). The values were corrected by the refractive index of the solvent. Radiative decay curves were registered with the time correlated single-photon counting technique as implemented in the aforementioned spectrofluorimeter. Fluorescence emission was monitored at the maximum emission wavelength after excitation at both visible absorption bands by means of a Fianium pulsed laser (time resolution of picoseconds) with tunable wavelength. The fluorescence lifetime (τ) was obtained after the deconvolution of the instrumental response signal from the recorded decay curves by means of an iterative method. The goodness of the exponential fit was controlled by statistical parameters (chi-square, Durbin-Watson and the analysis of the residuals).

Quantum mechanical calculations: Ground state geometries were optimized with the B3LYP hybrid functional, within the Density Functional Theory (DFT), using the double valence basis set with a polarization function (6-31G*), owing to the large molecular size of the cassettes, as implemented in the Gaussian 16. The geometries were considered as energy minimum when the corresponding frequency analysis did not give any negative value. Time-dependent method (TD-DFT) was used to evaluate the singlet and triplet manifold energetic distribution, and the singlet-triplet energy gap, from Franck-Condon transitions. To this aim CAM-B3LYP functional was used for a better description of long-range interactions (like charge transfer) and excitation energies. The solvent effect (ethyl acetate) was considered in all the above calculations by means of the Polarizable Continuum Model (PCM). Theodore software was used to estimate the charge transfer probability in the excited state at the same TD-DFT calculation level.

Electrochemistry: Cyclic voltammograms (Metrohm Autolab) were done using a threeelectrode set up with a platinum layer (surface 8 mm x 7.5 mm) working electrode, platinum wire as counter electrode and Ag/AgCl as reference electrode. A 0.1 M solution of tetrabutylammonium hexafluorophosphate (TBAPF6) in dry acetonitrile was used as the electrolyte solvent in which the compounds were dissolved to achieve a concentration of 0.5 mM. All redox potentials were reported vs ferrocene as internal standard. The solutions were purged with argon and all the measurements were performed under an inert atmosphere.

Laser properties: Laser efficiency was evaluated from concentrated solutions (milimolar) of dyes in ethyl acetate contained in 1-cm optical-path rectangular quartz cells carefully sealed to avoid solvent evaporation during experiments. The liquid solutions were transversely pumped with 8 mJ, 8 ns FWHM pulses from the third harmonic (355 nm) and the second harmonic (532 nm) of a Q-switched Nd:YAG laser (Lotis TII 2134) at a repetition rate of 1 Hz. The exciting pulses were line-focused onto the cell using a combination of positive and negative cylindrical lenses (f = 15 cm and f = -15 cm, respectively) perpendicularly arranged. The

plane parallel oscillation cavity (2 cm length) consisted of a 90% reflectivity aluminium mirror acting as back reflector, and the lateral face of the cell acting as output coupler (4% reflectivity). The pump and output energies were detected by a GenTec powermeter. The photostability of the dyes in ethyl acetate solution was evaluated by using a pumping energy and geometry exactly equal to that of the laser experiments. We used spectroscopic quartz cuvettes with 0.1 cm optical to allow for the minimum solution volume (V_S = 40 μL) to be excited. The lateral faces were grounded, whereupon no laser oscillation was obtained. Information about photostabilitiy was obtained by monitoring the decrease in laser-induced fluorescence (LIF) intensity. In order to facilitate comparisons independently of the experimental conditions and sample, the photostability figure of merit was defined as the accumulated pump energy absorbed by the system (E_{dose}), per mole of dye, before the output energy falls to a 10% its initial value. In terms of experimental parameters, this energy dose, in units of GJ mol^{-1}, can be expressed as:

$$E_{dose}^{50\%}(GJ\cdot mol^{-1}) = \frac{E_{pump}(GJ)\cdot\left(1-10^{-\varepsilon CL}\right)\cdot\sum_{\#pulses} f}{CV_S} \qquad (1)$$

where E_{pump} is the energy per pulse, C is the molar concentration, ε is the molar absorption coefficient in units of M^{-1} cm^{-1}, L is the depth of the cuvette expressed in cm, V_S is the solution volume, in litres, within the cuvette, and f is the ratio between the LIF intensity after #pulses and the LIF intensity in the first pulse. To speed up the experiment the pump repetition rate was increased up to 15 Hz. The fluorescence emission and laser spectra were monitored perpendicular to the exciting beam, collected by an optical fiber, and imaged onto a spectrometer (Acton Research corporation) and detected with a charge-coupled device (CCD) (SpectruMM:GS128B). The fluorescence emission was recorded by feeding the signal to the boxcar (Stanford Research, model 250) to be integrated before being digitized and processed by a computer. The estimated error in the energy and photostability measurements was 10%.

Delayed fluorescence. Aerated ethyl acetate solutions at room temperature of the new aza-BODIPY (**1-4** and its monomeric parent dye **8**) contained in 1-cm optical-path rectangular quartz cells was transversally pumped with intense laser pulses from the second (532 nm) and third (355 nm) harmonic of a Nd:YAG laser (LOTIS TII, LS-2147) at 10 Hz repetition rate. The emission was analyzed perpendicularly to the input radiation being focused onto a spectrograph (Kymera 193i-A, Andor Technologies) coupled to an intensified CCD camera (iStar, Andor Technologies). The camera enabled gate widths ranging from nanoseconds up to seconds and its opening can be delayed in a control way with respect to the incoming pump laser. The measurements were carried out for dye concentrations lower than 0.2 mM and energy fluences lower than 32 mJ/cm^2 to work well below the threshold for onset the laser action. Neither long-pass-filters nor band-pass filters were used to remove the excitation laser since we have verified that these filters, especially long pass filters, under drastic pump conditions, exhibited its own fluorescence and/or phosphorescence emission, which could lead to misunderstanding the experimental results. In addition, neither solvents (i.e. iodoethane) nor triplet sensitizers were added to the dye solution trying to enhance the triplet quantum yield. Each spectrum is the average of 200 scans recorded with a gate time of 50 μs.

2. Synthesis and characterization

2.1. General procedure for Suzuki Miyaura reaction.

Method A: To a solution of the corresponding halogenated *aza*-BODIPY (1 equiv) and pinacol boronate BODIPY (3 equiv) in toluene/THF/water (1:1:1, v/v/v) was added Na_2CO_3 (4 equiv) and argon was bubbled through the solution for 30 min. Then, $Pd(PPh_3)_4$ (10% mol) was added and the mixture was heated at 80 ºC under argon atmosphere for 10 h. After removal of the solvent under reduced pressure, the reaction mixture was diluted with CH_2Cl_2 and washed with water. The organic layer was dried over Na_2SO_4, filtered and evaporated to dryness. The crude product was purified by flash chromatography on silica gel.

Method B: To a solution of the corresponding halogenated *aza*-BODIPY (1 equiv) and pinacol boronate BODIPY (3 equiv) in toluene/THF/water (1:1:1, v/v/v) were added K_2CO_3

(4 equiv) and $Pd(PPh_3)_4$ (10% mol) in argon atmosphere, and the mixture was heated under microwave irradiation (Biotage® Initiator Classic) at 120 ºC for 1 h. After removal of the solvent under reduced pressure, the reaction mixture was diluted with CH_2Cl_2 and washed with water. The organic layer was dried over Na_2SO_4, filtered and evaporated to dryness. The crude product was purified by flash chromatography on silica gel.

2.2. General procedure for the synthesis of O-aza-BODIPYs. To a solution of *aza*-BODIPY (1 equiv) in dry CH_2Cl_2 was added aluminium chloride (2 equiv) under an argon atmosphere and the mixture resulting was refluxed for 5-10 min. Then, 8-(4-hydroxyphenyl)BODIPY (5 equiv) was added and the mixture was refluxed until the complete consumption of the starting material was observed by TLC. Water was added, and the solution was extracted with CH_2Cl_2, dried over Na_2SO_4, filtered and concentrated to dryness. The compounds were purified by flash chromatography on silica gel.

2.3. Synthesis of cassettes

Cassette 1:

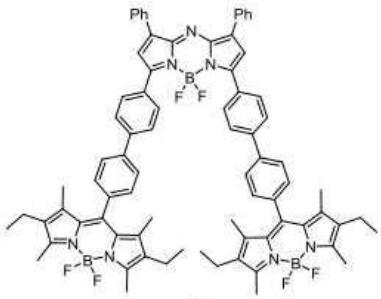

1

According to the general procedure 2.1., method A, *aza*-BODIPY **5**[1] (38 mg, 0.058 mmol), pinacol boronate BODIPY **6**[2] (88 mg, 0.174 mmol), Na_2CO_3 (25 mg, 0.232 mmol), $Pd(PPh_3)_4$ (6.7 mg, 0.006 mmol) in toluene/THF/water (1:1:1, 15 mL) were reacted for 10 h. Flash chromatography using hexane/CH_2Cl_2 (70:30 to 40:60) afforded **1** (19 mg, 26%) as a green solid. ^{1}H NMR (700 MHz, $CDCl_3$) δ 8.23 (d, J = 8.4 Hz, 4H, 4CH), 8.11 (d, J = 7.0 Hz, 4H, 4CH), 7.85 (d, J = 8.4 Hz, 4H, 4CH), 7.82 (d, J = 7.7 Hz, 4H, 4CH), 7.52-7.46 (m, 6H, 6CH), 7.39 (d, J = 7.7 Hz, 4H, 4CH), 7.16 (s, 2H, 2CH), 2.55 (s, 12H, $4CH_3$), 2.31 (q, J = 7.7 Hz, 8H, $4CH_2$), 1.35 (s, 12H, $4CH_3$), 0.99 (t, J = 7.7 Hz, 12H, $4CH_3$) ppm. ^{13}C NMR (176 MHz, $CDCl_3$) δ 158.7 (C), 153.9 (C), 145.9 (C), 144.3 (C), 142.3 (C), 140.3 (C), 139.6 (C), 138.3 (C), 135.6 (C), 132.9 (C), 132.3 (C), 131.0 (C), 130.7 (C), 130.4 (CH), 129.7 (CH), 129.4 (CH), 129.0 (CH), 128.7 (CH), 127.6 (CH), 127.2 (CH), 119.2 (CH), 17.1 (CH_2), 14.7

(CH_3), 12.6 (CH_3), 11.9 (CH_3) ppm. FTIR ν 2959, 2921, 2852, 1606, 1507, 1320, 1193, 1115, 1071, 1040, 980, 945 cm^{-1}. HRMS MALDI-TOF (*m/z*) 1253.9022 (1253.9034 calcd. for $C_{78}H_{72}B_3F_6N_7$).

Cassettes 2a and 2b.

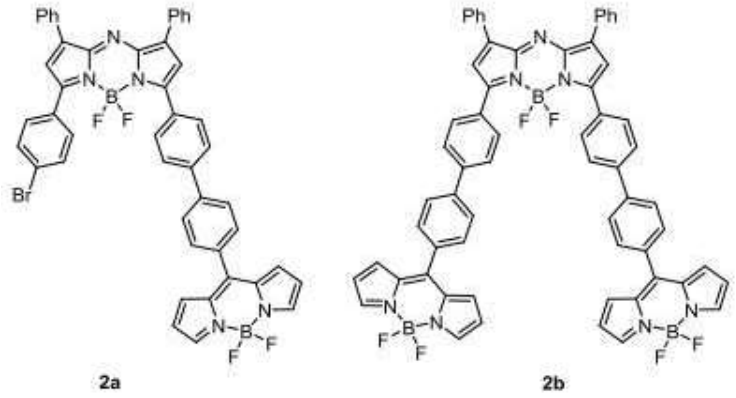

2a: According to the general procedure 2.1., method A, *aza*-BODIPY **5**[1] (60 mg, 0.091 mmol), pinacol boronate BODIPY **7**[3] (108 mg, 0.273 mmol), Na_2CO_3 (39 mg, 0.364 mmol), $Pd(PPh_3)_4$ (11.1 mg, 0.009 mmol) in toluene/THF/water (1:1:1, 6 mL) were reacted for 20 h. Flash chromatography using hexane/EtOAc (85:15 to 60:40) afforded **2a** (59 mg, 77%) as a green solid**.** ^{1}H NMR (700 MHz, $CDCl_3$) δ 8.23 (d, J = 8.4 Hz, 2H, 2CH), 8.09 (d, J = 7.0 Hz, 2H, 2CH), 8.07 (d, J = 7.0 Hz, 2H, 2CH), 7.98 (s, 2H, 2CH), 7.95 (d, J = 8.4 Hz, 2H, 2CH), 7.83 (d, J = 8.4 Hz, 2H, 2CH), 7.82 (d, J = 8.4 Hz, 2H, 2CH), 7.70 (d, J = 8.4 Hz, 2H, 2CH), 7.64 (d, J = 8.4 Hz, 2H, 2CH), 7.51-7.45 (m, 6H, 6CH), 7.16 (s, 1H, CH), 7.03 (br s, 3H, 3CH), 6.59-6.58 (m, 2H, 2CH) ppm. ^{13}C NMR (176 MHz, $CDCl_3$) δ 159.1 (C), 157.9 (C), 146.8 (C), 146.1 (C), 145.7 (C), 144.8 (C), 144.3 (C), 144.2 (CH), 142.6 (C), 142.2 (C), 134.9 (C), 133.5 (C), 132.2 (C), 132.1 (C), 132.0 (CH), 131.6 (CH), 131.3 (CH), 131.2 (C), 131.0 (CH), 130.53 (C), 130.46 (CH), 129.8 (CH), 129.7 (CH), 129.5 (CH), 129.4 (CH), 128.8 (CH), 128.7 (CH), 127.5 (CH), 127.2 (CH), 125.9 (C), 119.4 (CH), 118.8 (CH), 118.7 (CH) ppm. FTIR ν 2934, 2921, 2853, 1556, 1534, 1509, 1474, 1412, 1387, 1261, 1115, 1077, 1038, 981 cm^{-1}. HRMS-MALDI-TOF (*m/z*) 841.1795 (841.1807 calcd. for $C_{47}H_{30}B_2BrF_4N_5$).

2b: According to the general procedure 2.1., method B, *aza*-BODIPY **5**[1] (71 mg, 0.108 mmol), pinacol boronate BODIPY **7**[3] (128 mg, 0.324 mmol), K_2CO_3 (60 mg, 0.432 mmol), $Pd(PPh_3)_4$ (12.6 mg, 0.011 mmol) in toluene/THF/water (1:1:1, 5 mL) were reacted for 1 h. Flash chromatography using hexane/CH_2Cl_2/EtOAc (77:20:3 to 45:35:20) afforded **2b** (44 mg,

40%) as a green solid**.** ^{1}H NMR (700 MHz, $CDCl_3$) δ 8.26 (d, J = 8.4 Hz, 4H, 4CH), 8.12 (d, J = 7.0 Hz, 4H, 4CH), 7.97 (s, 4H, 4CH), 7.83 (d, J = 8.4 Hz, 4H, 4CH), 7.82 (d, J = 7.7 Hz, 4H, 4CH), 7.69 (d, J = 7.7 Hz, 4H, 4CH), 7.52-7.46 (m, 6H, 6CH), 7.17 (s, 2H, 2CH), 7.02 (d, J = 4.2 Hz, 4H, 4CH), 6.58 (d, J = 4.2 Hz, 4H, 4CH) ppm. ^{13}C NMR (176 MHz, $CDCl_3$) δ 158.7 (C), 146.8 (C), 146.0 (C), 144.5 (C), 144.2 (CH), 142.6 (C), 142.0 (C), 134.9 (C), 132.2 (C), 131.5 (CH), 131.35 (C), 131.28 (CH), 130.4 (CH), 129.8 (CH), 129.5 (CH), 128.8 (CH), 127.4 (CH), 127.2 (CH), 119.3 (CH), 118.7 (CH) ppm. FTIR ν 2923, 2851, 1556, 1532, 1505, 1474, 1411, 1386, 1259, 1225, 1075, 1037 cm^{-1}. HRMS-MALDI-TOF (*m/z*) 1029.3516 (1029.3529 calcd. for $C_{62}H_{40}B_3F_6N_7$).

Cassette 3:

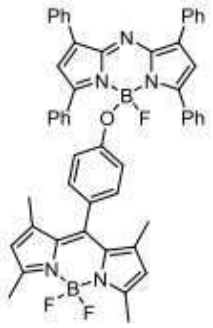

3

According to the general procedure 2.2., *aza*-BODIPY **8**[4] (30 mg, 0.060 mmol), 8-(4-hydroxyphenyl)-1,3,5,7-tetramethylBODIPY **9**[5] (102 mg, 0.300 mmol), $AlCl_3$ (16 mg, 0.120 mmol) in CH_2Cl_2 (15 mL) were reacted for 3 h. Flash chromatography using hexane/EtOAc (95:5 to 50:50) afforded **3** (16 mg, 33%) as a green solid, and recupered **8** (7 mg, 23%)**.** ^{1}H NMR (700 MHz, $CDCl_3$) δ 8.07 (d, J = 7.0 Hz, 4H, 4CH), 8.02 (d, J = 7.0 Hz, 4H, 4CH), 7.48-7.44 (m, 12H, 12CH), 7.01 (s, 2H, 2CH), 6.68 (d, J = 9.1 Hz, 2H, 2CH), 6.16 (d, J = 9.1 Hz, 2H, 2CH), 5.85 (s, 2H, 2CH), 2.47 (s, 6H, $2CH_3$), 1.14 (s, 6H, $2CH_3$) ppm. ^{13}C NMR (176 MHz, $CDCl_3$) δ 160.2 (C), 156.3 (d, $^{3}J_{CF}$ = 7.0 Hz, C), 155.2 (C), 145.9 (C), 144.5 (C), 143.4 (C), 142.6 (C), 132.5 (C), 132.0 (C), 131.9 (C), 131.2 (CH), 130.22 (CH), 130.20 (CH), 130.0 (CH), 129.7 (CH), 129.0 (CH), 128.7 (CH), 128.6 (CH), 126.7 (C), 121.1 (CH), 119.7 (CH), 119.4 (CH), 14.8 (CH_3), 14.7 (CH_3) ppm. FTIR ν 2922, 2855, 1590, 1510, 1445, 1380, 1261, 1120, 1071 cm^{-1}. HRMS-MALDI-TOF (*m/z*) 817.3359 (817.3371 calcd. for $C_{51}H_{40}B_2F_3N_5O$).

Cassettes 4a and 4b:

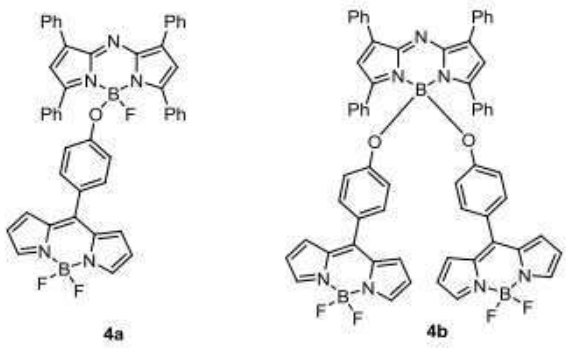

According to the general procedure 2.2., *aza*-BODIPY **8**[4] (50 mg, 0.100 mmol), 8-(4-hydroxyphenyl)BODIPY **10**[6] (142 mg, 0.500 mmol), AlCl3 (27 mg, 0.200 mmol) in CH_2Cl_2 (15 mL) were reacted for 3 h. Flash chromatography using hexane/EtOAc (90:10 to 75:25) afforded **4a** (15 mg, 20%) and **4b** (26 mg, 25%) as green solids.

4a:. ^{1}H NMR (700 MHz, $CDCl_3$) δ 8.10 (d, J = 7.0 Hz, 4H, 4CH), 7.99 (d, J = 7.0 Hz, 4H, 4CH), 7.83 (s, 2H, 2CH), 7.50-7.44 (m, 12H, 12CH), 7.07 (d, J = 9.1 Hz, 2H, 2CH), 7.01 (s, 2H, 2CH), 6.76 (d, J = 3.5 Hz, 2H, 2CH), 6.44-6.44 (m, 2H, 2CH), 6.17 (d, J = 9.1 Hz, 2H, 2CH) ppm. ^{13}C NMR (176 MHz, $CDCl_3$) δ 160.0 (C), 158.7 (d, $^3J_{CF}$ = 7.0 Hz, C), 147.9 (C), 145.6 (C), 144.3 (C), 142.9 (CH), 134.6 (C), 132.1 (C), 132.0 (CH), 131.6 (C), 131.3 (CH), 130.9 (CH), 129.93 (CH), 129.91 (CH), 129.8 (CH), 129.4 (CH), 128.8 (CH), 128.4 (CH), 125.5 (C), 119.4 (CH), 118.8 (CH), 117.9 (CH) ppm. FTIR ν 2920, 2851, 1600, 1514, 1454, 1412, 1387, 1261, 1119, 1075 cm^{-1}. HRMS-MALDI-TOF (*m/z*) 761.2727 (761.2745 calcd. for $C_{47}H_{32}B_2F_3N_5O$).

4b: ^{1}H NMR (700 MHz, $CDCl_3$) δ 8.05-8.03 (m, 4H, 4CH), 8.01 (d, J = 7.0 Hz, 4H, 4CH), 7.85 (s, 2H, 2CH), 7.51-7.44 (m, 12H, 12CH), 7.21 (d, J = 9.1 Hz, 4H, 4CH), 7.02 (s, 2H, 2CH), 6.79 (d, J = 4.2 Hz, 4H, 4CH), 6.51 (d, J = 9.1 Hz, 4H, 4CH), 6.44 (dd, J = 4.2 and 2.1 Hz, 4H, 4CH) ppm. ^{13}C NMR (176 MHz, $CDCl_3$) δ 160.3 (C), 158.6 (C), 147.8 (C), 145.7 (C), 144.3 (C), 143.1 (CH), 134.7 (C), 132.1 (CH), 131.9 (C), 131.6 (C), 131.3 (CH), 131.0 (CH), 130.2 (CH), 130.0 (CH), 129.4 (CH), 128.8 (CH), 128.3 (CH), 126.1 (C), 120.0 (CH), 119.4 (CH), 118.0 (CH) ppm. FTIR ν 2921, 2850, 1599, 1538, 1510, 1475, 1412, 1387, 1261, 1116, 1075, 1036 cm^{-1}. HRMS-MALDI-TOF (*m/z*) 742.2776 [M-$C_{15}H_{10}BF_2N_2O$] (1025.3615 calcd. for $C_{62}H_{42}B_3F_4N_7O_2$).

3. Photophysical data. Figures S1 and S2

Table S1. Photophysical properties of aza-BODIPY-based energy transfer cassettes dissolved (2 μM) in apolar and polar media.

Dye solvent	λ_{ab} [a] (nm)	ε_{max} [b] (10^4 $M^{-1}\cdot cm^{-1}$)	λ_{fl} [c] (nm)	ϕ [d]	τ [e] (ns)	k_{fl} [f] ($10^8 s^{-1}$)	k_{nr} [g] ($10^8 s^{-1}$)
1*							
c-hex	675.5	4.8	710.5	0.01	1.87	0.05	5.30
	525.5	10.4					
EtOAc	678.5	6.7	711.5	0.006	NR	-	-
	523.0	12.1					
2a							
c-hex	663.5	7.2	693.0	0.25	1.72	1.45	4.36
	503.0	6.0					
EtOAc	667.5	7.7	701.0	0.24	1.83	1.31	4.15
	500.5	5.7					
MeOH	664.5	7.3	697.5	0.18	1.36	1.32	6.03
	499.5	5.6					
2b[#]							
EtOAc	680.0	10.4	718.5	0.30	2.28	1.31	3.07
	500.5	13.9					
3							
c-hex	643.0	2.7	669.5	0.08	0.51(34%) – 1.28(66%)	-	-
	501.5	4.0					
EtOAc	651.5	3.9	672.5	0.007	NR	-	-
	497.5	5.3					
MeOH	647.5	2.9	674.0	0.02	0.05(65%) – 0.39(35%)	-	-
	497.0	4.4					
4a							
c-hex	647.5	7.7	675.0	0.09	0.86	1.04	10.6
	497.5	7.4					
EtOAc	649.5	8.2	675.0	0.08	0.84	0.95	10.9
	494.5	7.7					
MeOH	646.0	7.7	675.0	0.05	0.58	0.86	16.4
	494.0	6.8					
4b							
c-hex	649.0	3.5	678.0	0.09	1.32	0.68	6.90
	498.0	7.7					
EtOAc	655.0	7.2	678.5	0.08	1.03	0.77	8.93
	494.5	13.3					
MeOH	651.5	5.5	676.0	0.05	0.71	0.70	13.4
	494.0	10.1					

[a]Absorption wavelength; [b]Extinction coefficient of the main maxima; [c]Fluorescence wavelength; [d]Fluorescence quantum yield; [e]Fluorescence lifetime (independent of the excitation); [f]Radiative rate constant; [g]Non-radiative rate constant.

NR: non-recorded because they are below 50 ps, the time-resolution of the photon counter

c-hex: cyclohexane. EtOAc: ethyl acetate. MeOH: methanol.

*not soluble in methanol. [#]not soluble in cyclohexane and methanol.

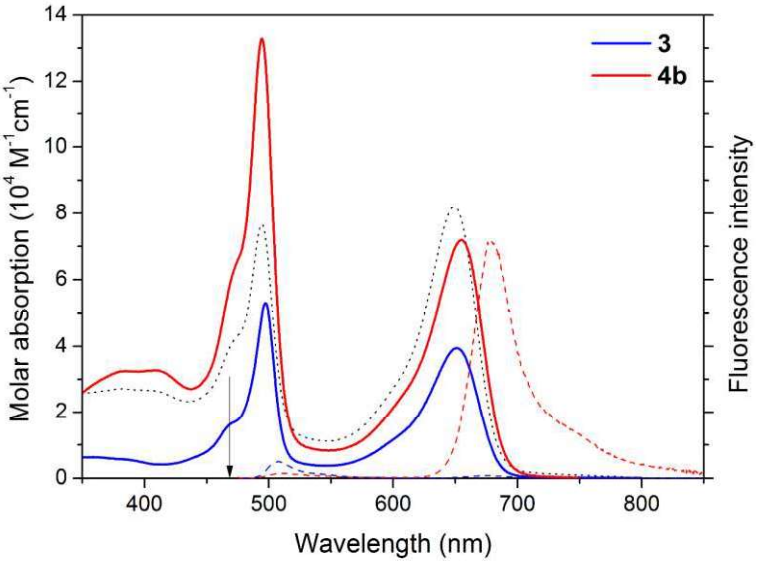

Figure S1. Absorption and fluorescence (dashed, after selective excitation of the BODIPY, see the arrow) spectra of the cassettes linked through a biphenyl spacer (**3** and **4b**). The corresponding absorption spectrum of **4a** (dotted line in black) is also added to show the effect of the number of energy donor units.

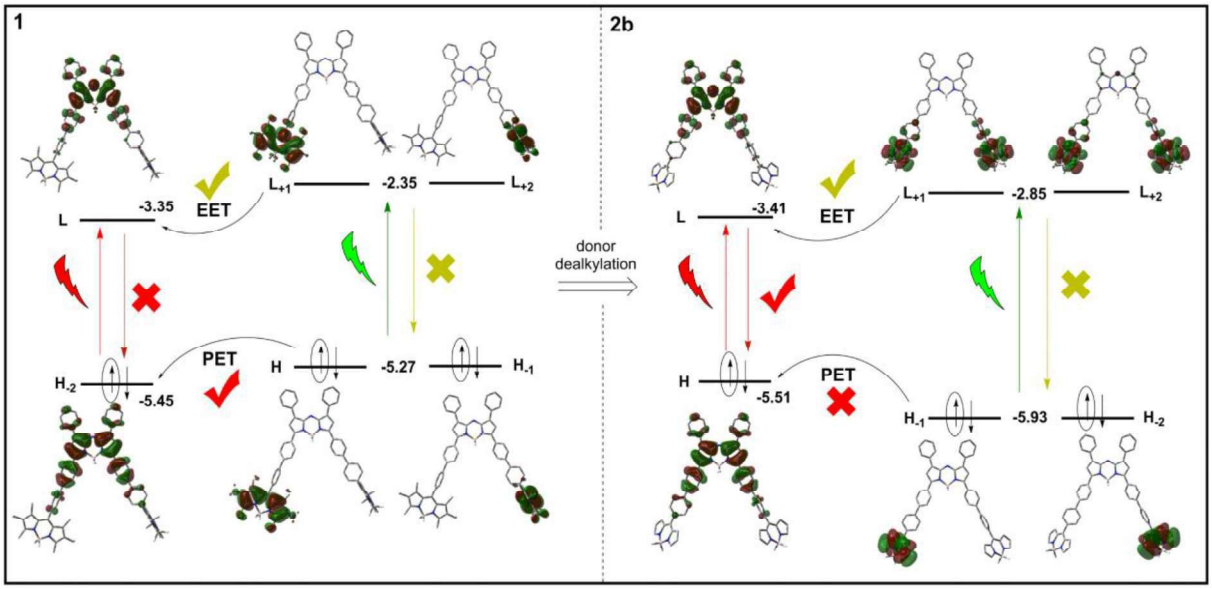

Figure S2. Computed molecular orbitals (b3lyp/6-31g*) and energies from the analogs **1** and **2b** just differing in the alkylation of the BODIPY energy donor tethered at the 3,5-biphenyl moiety of the aza-BODIPY core. The probability of the competing fluorescence, EET and PET processes is depicted.

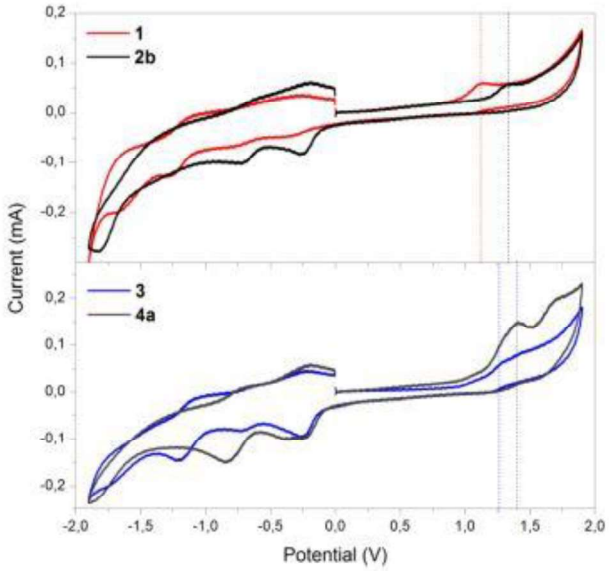

Figure S3. Cyclic voltammograms (positive scan, 0.2 V/s) of aza-BODIPY-based cassettes 2b and 4a, and their respective analogs bearing alkylated BODIPY energy donors (**1** and **3**, respectively), in acetonitrile (0.5 mM), using TBAPF& 0.1 M as electrode.

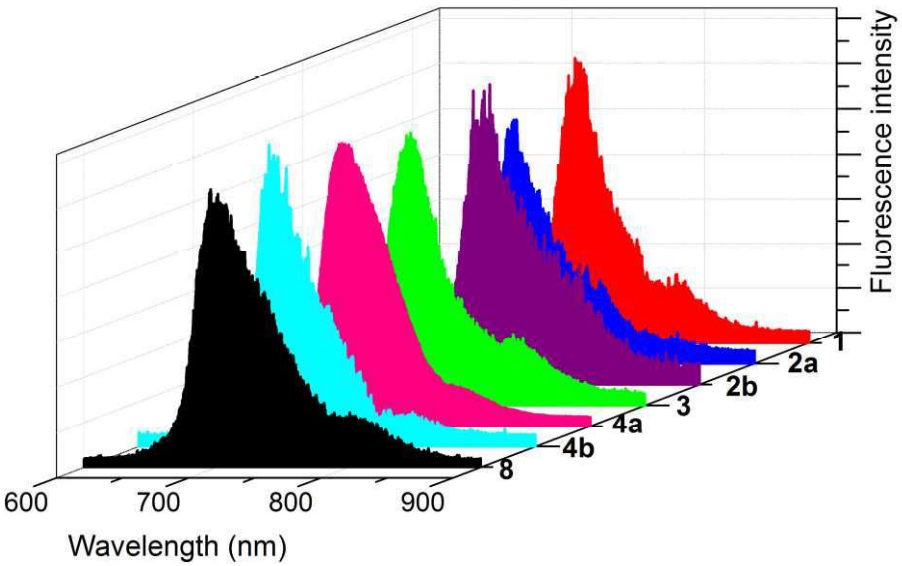

Figure S4. Delayed fluorescence spectra of the new aza-BODIPY cassettes (**1-4**) in aerated ethyl acetate solution (0.1 mM) at room temperature recorded with a delay of 50 μs with respect the incoming laser radiation (532 nm and 20 mJ/cm^2 fluence). For comparison the delayed fluorescence spectrum of the monomeric dye **8** recorded under identical experimental conditions is also included.

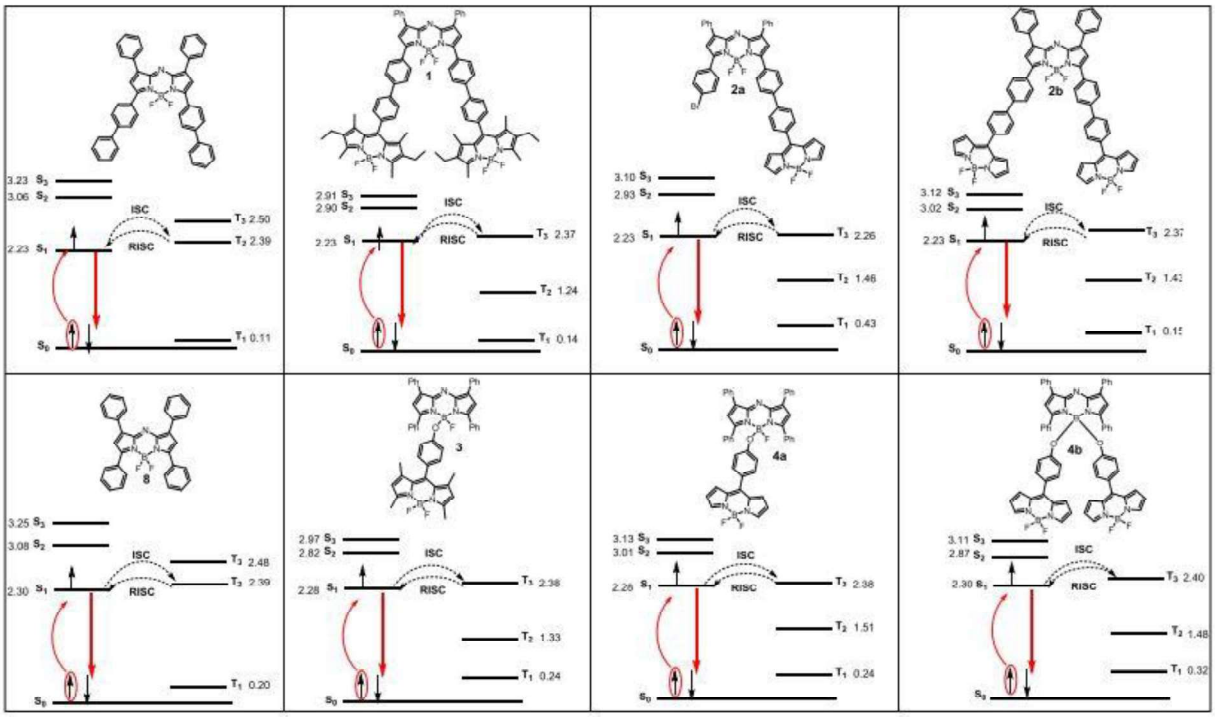

Figure S5.- Computed (td cam-b3lyp/6-31g*) singlet and triplet manifold energies (in eV) calculated as Franck-Condon transitions from the optimized ground state geometry of the isolated BODIPY energy donor and aza-BODIPY acceptor as well as the derived cassettes.

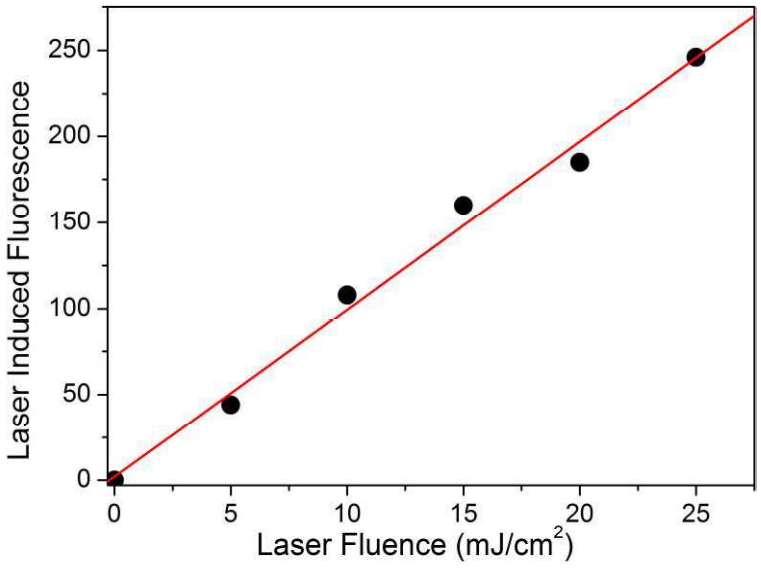

Figure S6.- Dependence on the laser fluence at 532 nm of the delayed fluorescence of **2b** in aerated ethyl acetate solution (0.1 mM) at room temperature recorded at a delay time of 10 μs. The solid line is the best fit of the data points (fit parameters: slope: 0.99517, χ^2 <0.0001).

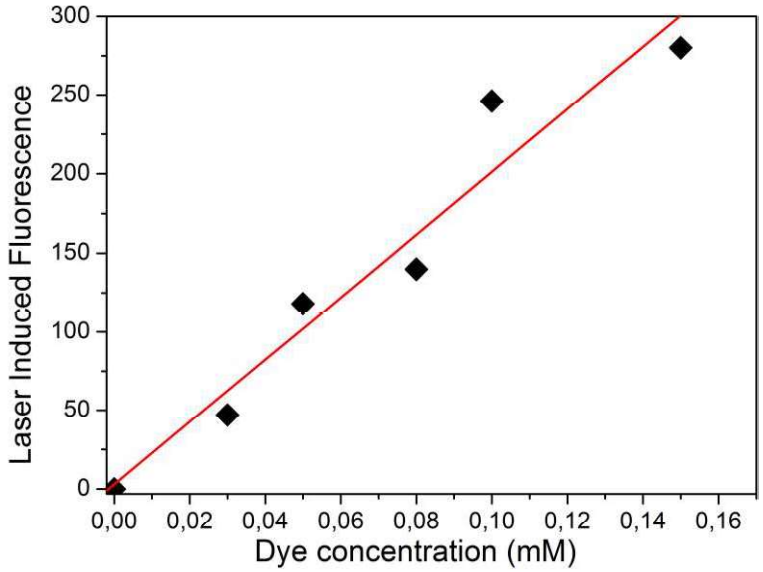

Figure S7.- Dependence on the dye concentration of the delayed fluorescence of **2b** in aerated ethyl acetate solution at room temperature recorded at a delay time of 10 μs with respect to the incoming radiation (532 nm, 25 mJ/cm^2). The solid line is the best fit of the data points (fit parameters: slope: 0.971, χ^2 <0.00123).

4. ^{1}H NMR and ^{13}C NMR spectra

^{1}H NMR (700 MHz, $CDCl_3$) and ^{13}C NMR (176 MHz, $CDCl_3$) spectra of **1**

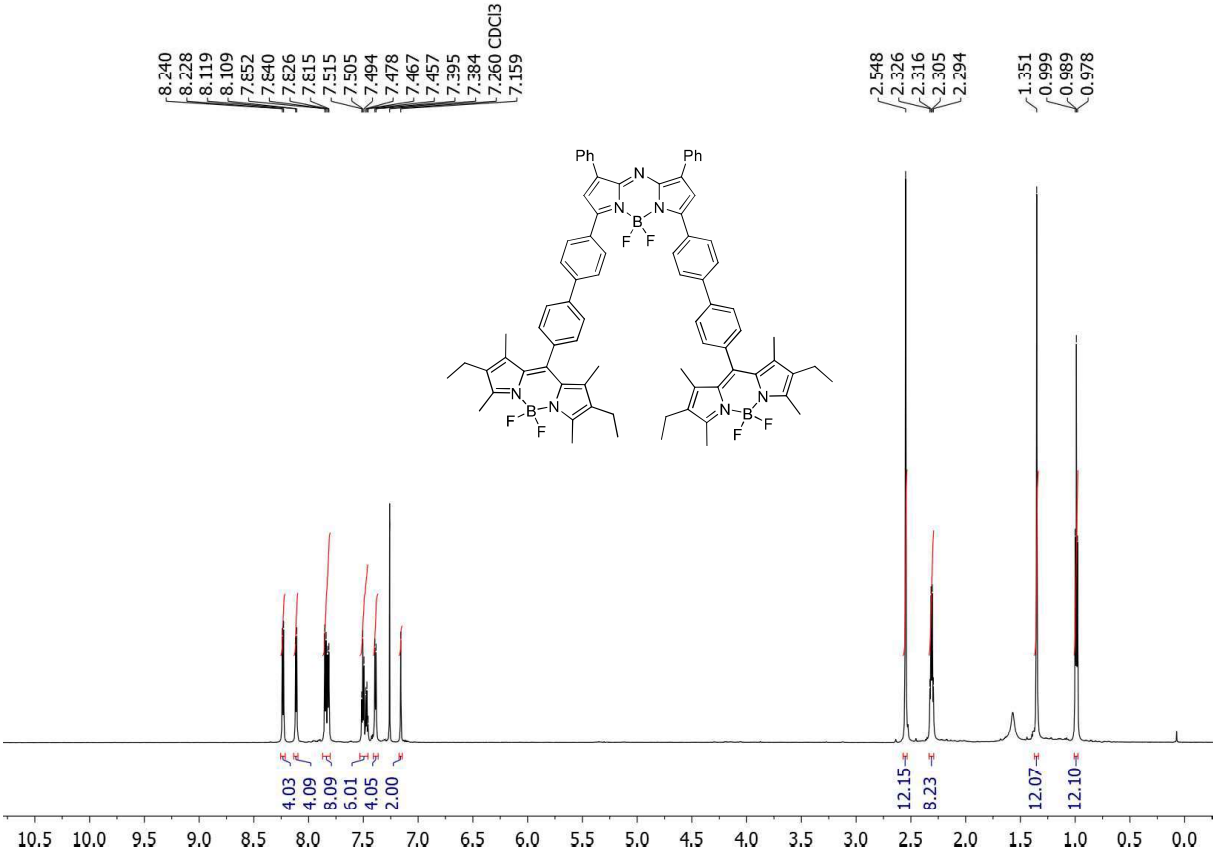

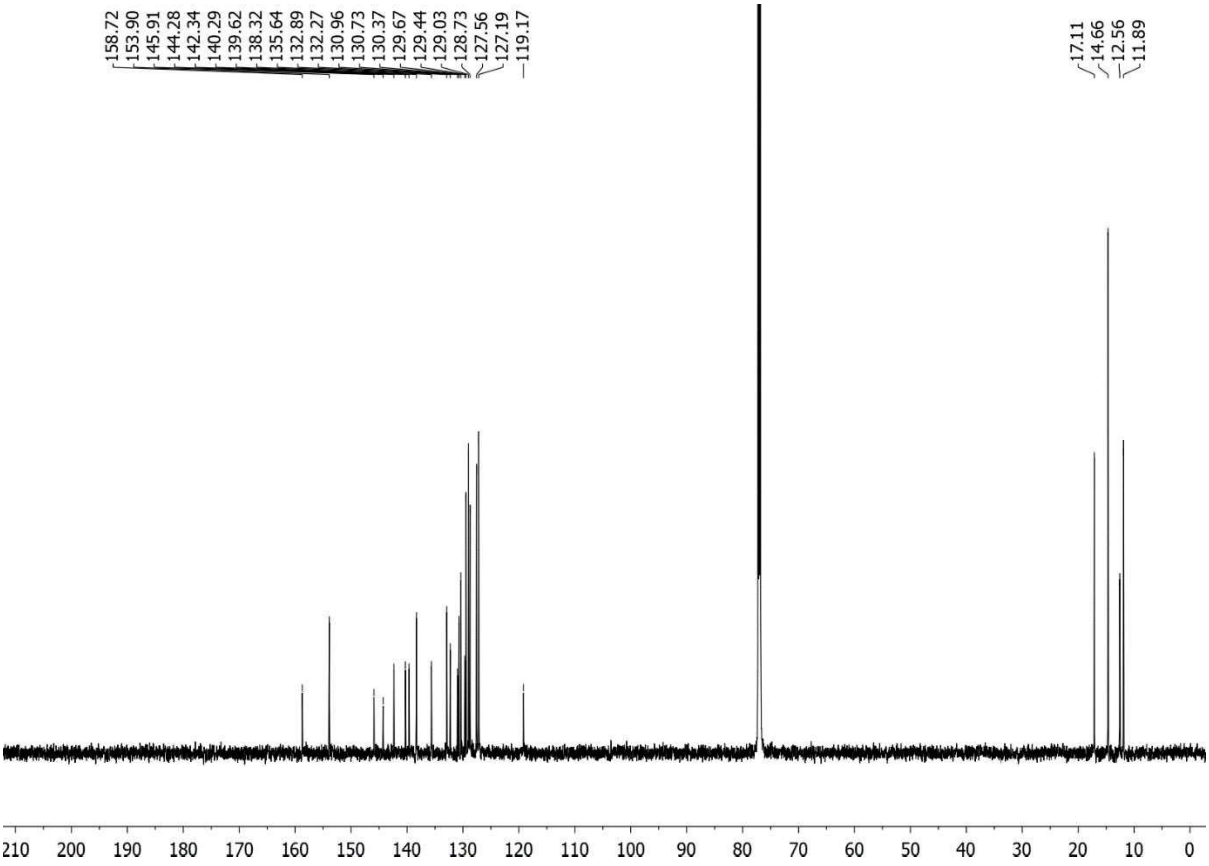

^{1}H NMR (700 MHz, $CDCl_3$) and ^{13}C NMR (176 MHz, $CDCl_3$) spectra of **2a**

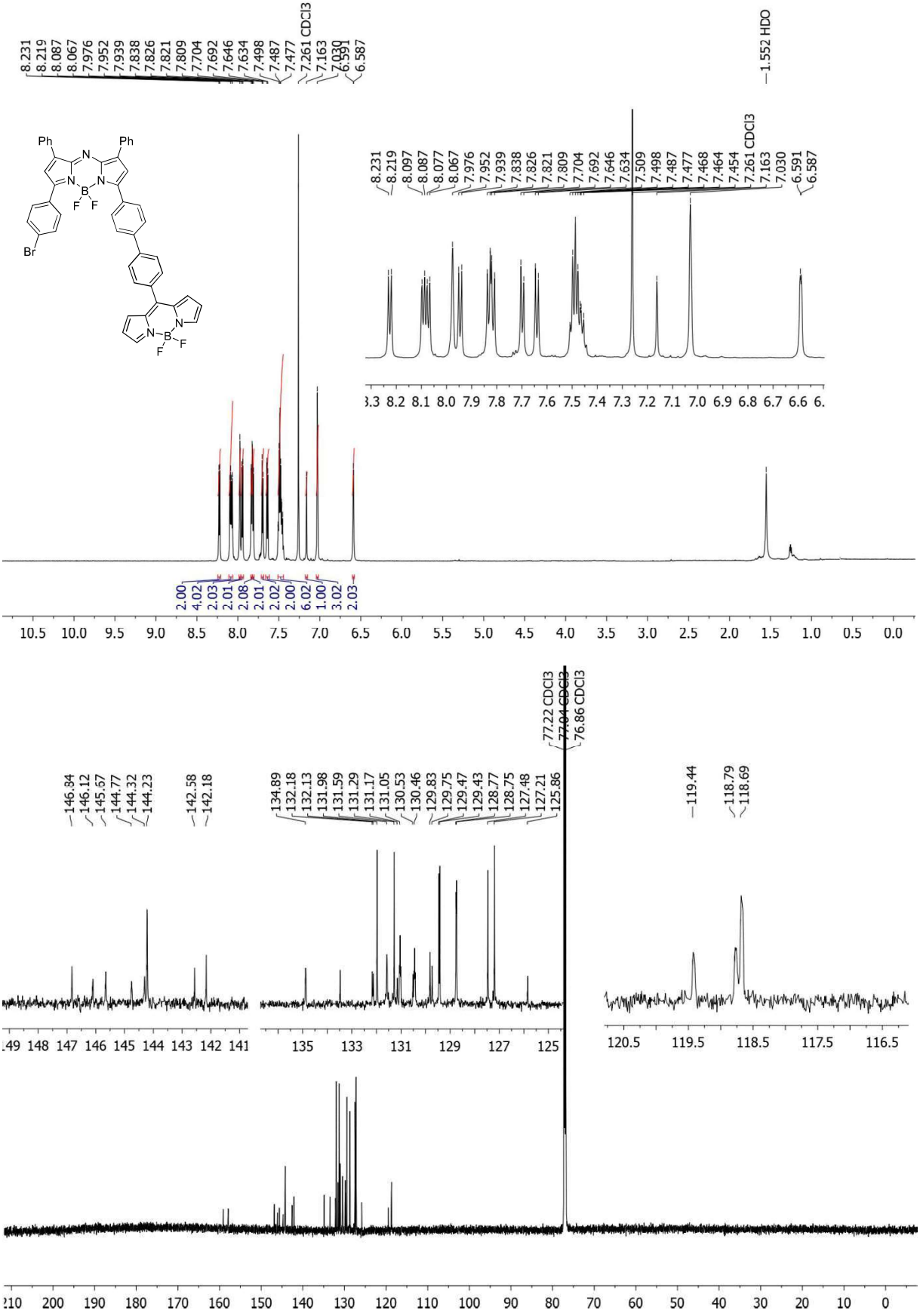

^{1}H NMR (700 MHz, $CDCl_3$) and ^{13}C NMR (176 MHz, $CDCl_3$) spectra of **2b**

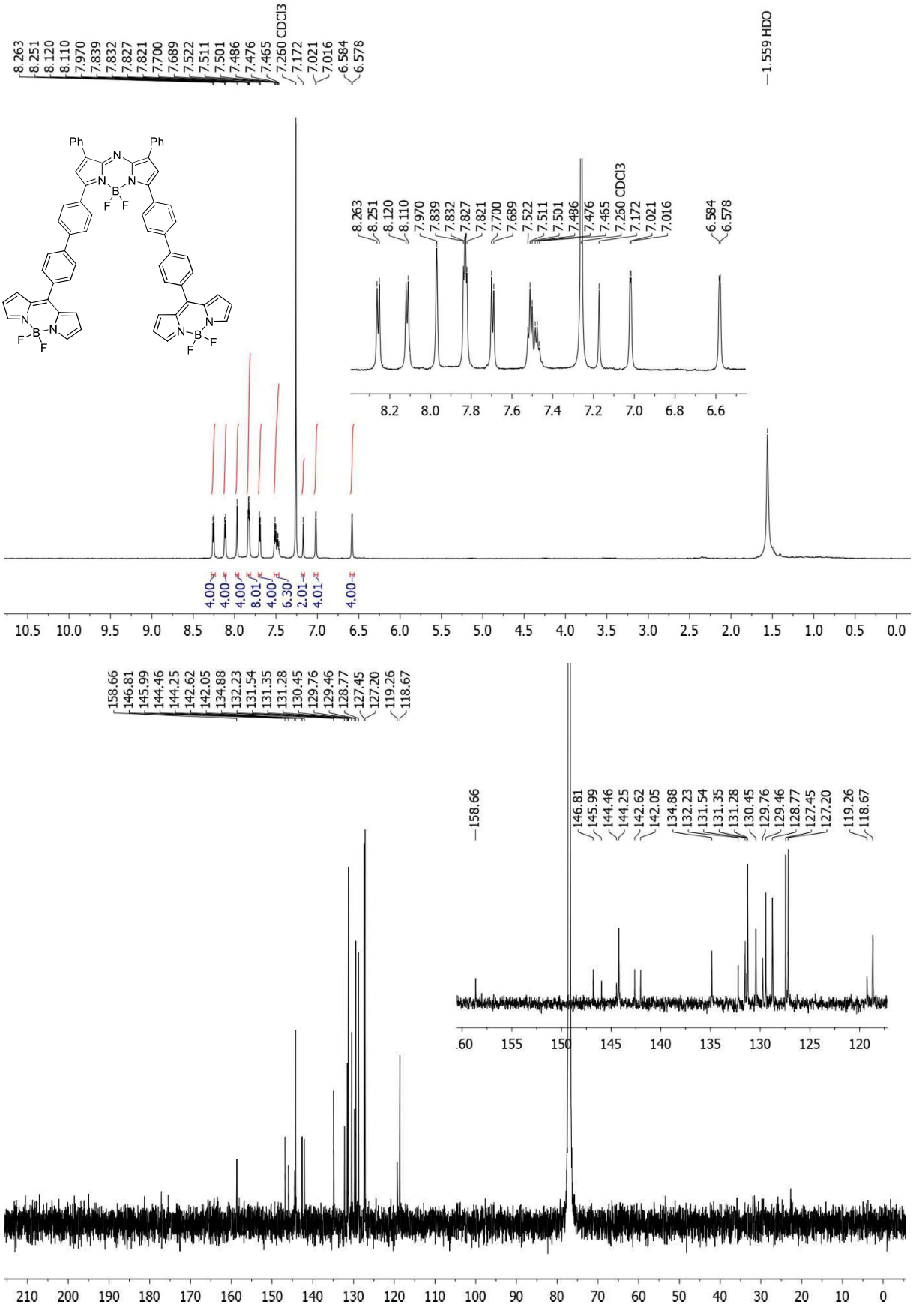

^{1}H NMR (700 MHz, $CDCl_3$) and ^{13}C NMR (176 MHz, $CDCl_3$) spectra of **3**

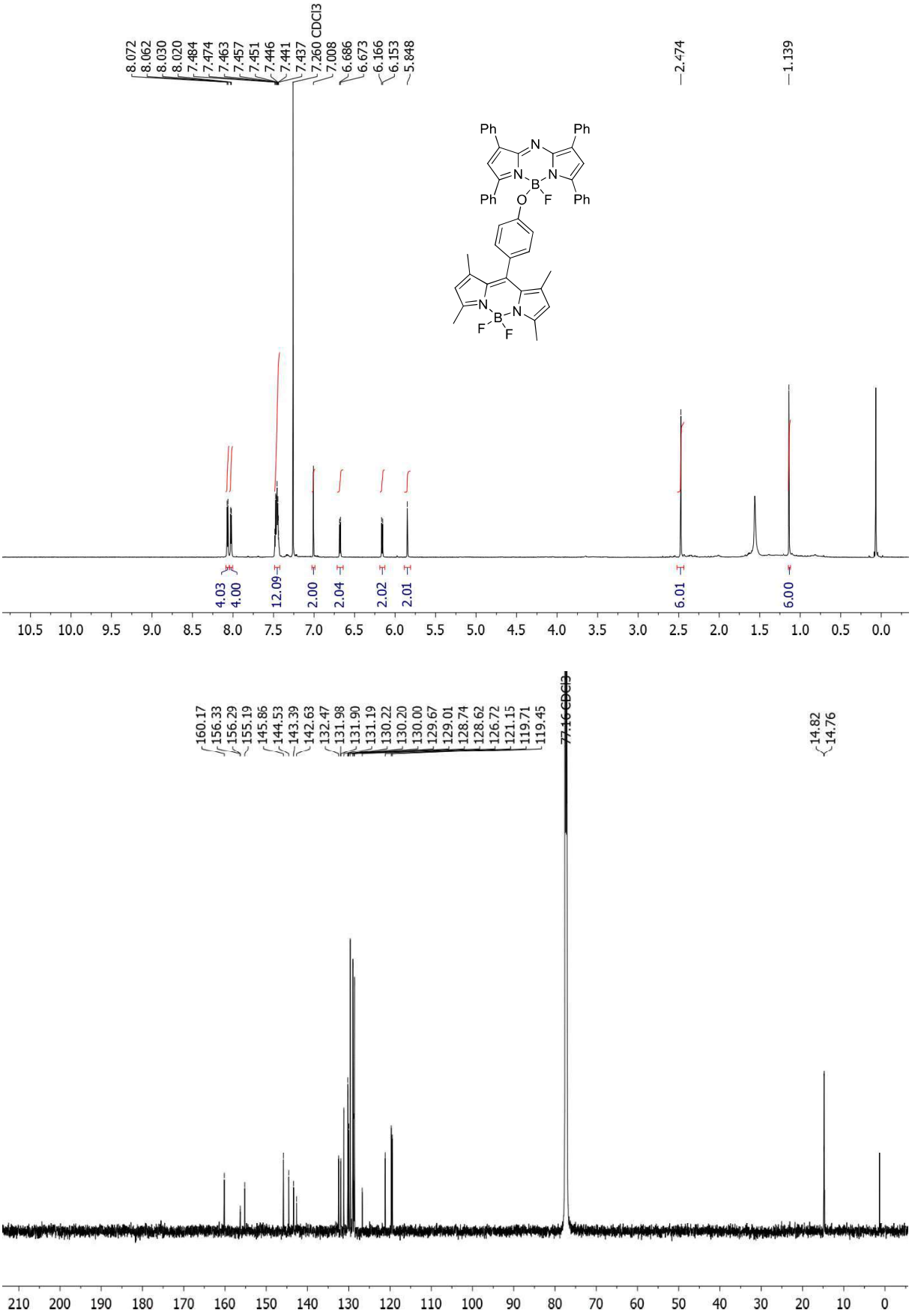

^{1}H NMR (700 MHz, $CDCl_3$) and ^{13}C NMR (176 MHz, $CDCl_3$) spectra of **4a**

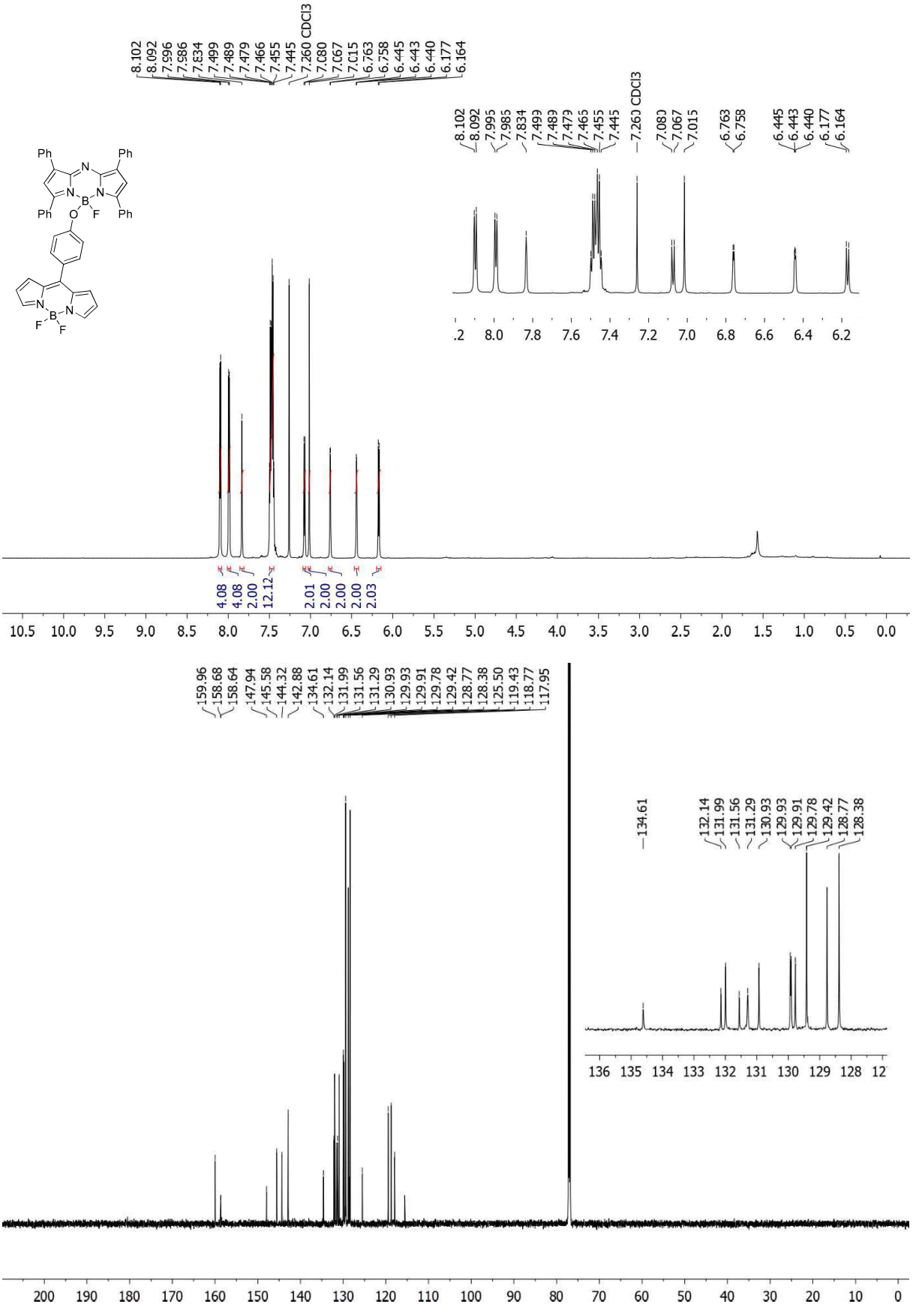

^{1}H NMR (700 MHz, $CDCl_3$) and ^{13}C NMR (176 MHz, $CDCl_3$) spectra of **4b**

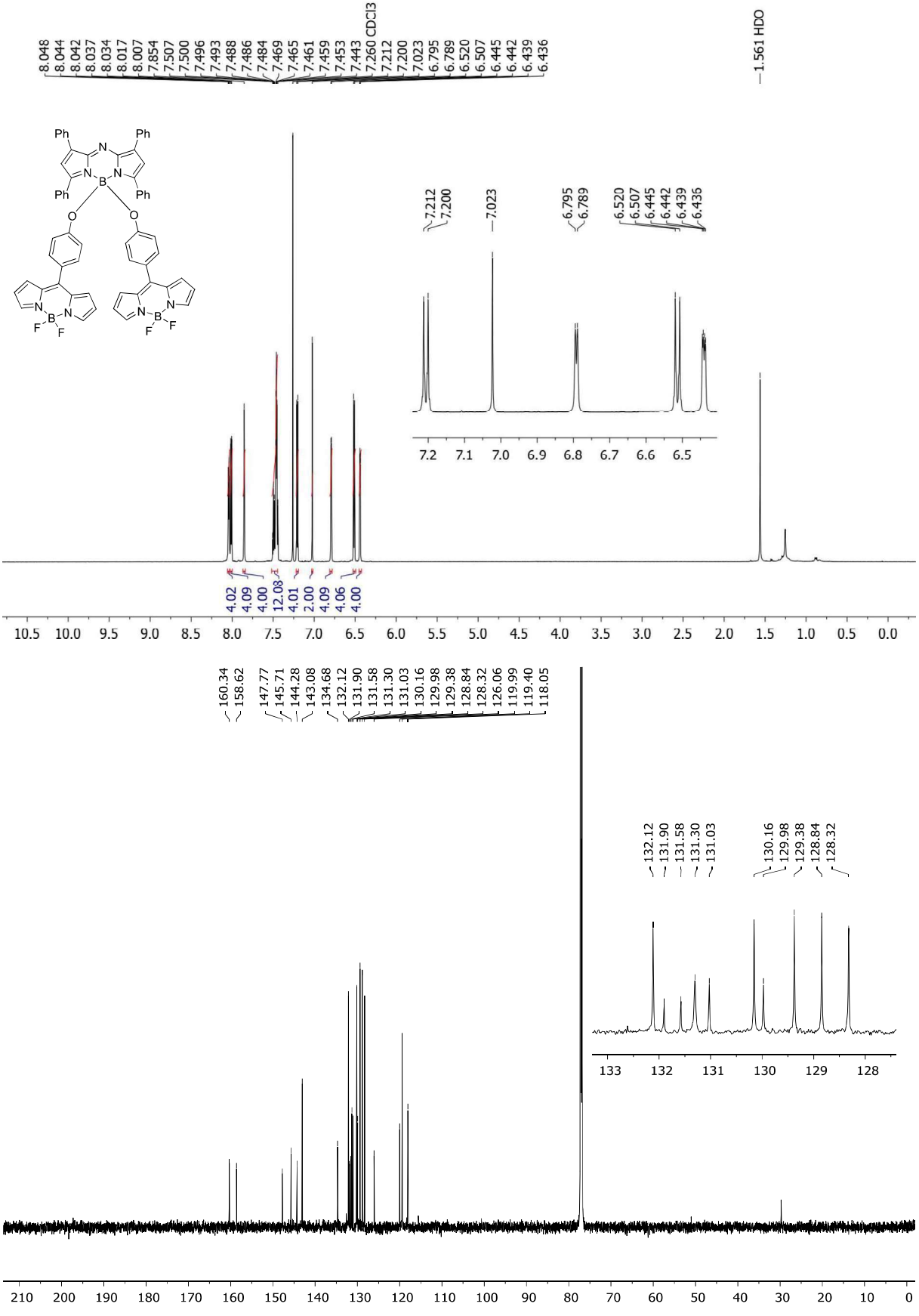

5. Cartesian coordinates. Table S2

Table S2. Atom coordinates and total energy (in hartrees) in the ground state (b3lyp/6-31g*) for aza-BODIPY **8** and its derived multichromophoric energy transfer cassettes after anchoring BODIPY energy donors at the 3,5-phenyls (**1** and **2a-b**) or at the boron bridge (**3** and **4a-b**).

1	C	0.39211082	7.28382013	-0.16195483
	N	0.64601810	5.91065491	-0.18625940
	B	-0.50330381	4.84388428	-0.09704855
	N	-1.85122512	5.64898269	-0.04633919
	C	-1.89049367	7.04286911	-0.12763568
	N	-0.81822403	7.81420756	-0.15823880
	C	-3.14096152	5.20117572	-0.08761149
	C	-4.01485765	6.31584196	-0.16265308
	C	-3.26125090	7.48054199	-0.18503630
	C	1.64028097	8.00088208	-0.12854100
	C	2.62148394	7.02000823	-0.10674949
	C	2.00091053	5.74504720	-0.13278610
	F	-0.53682938	4.02852422	-1.22560313
	F	-0.30496686	4.10041149	1.06390905
	C	-3.76188892	8.85727555	-0.24052070
	C	1.84079132	9.45306214	-0.13290335
	C	-5.04777822	9.15042689	0.25568738
	C	-5.56070460	10.44306848	0.19589276
	C	-4.80109366	11.47453728	-0.36239145
	C	-3.52462103	11.19927605	-0.85754634
	C	-3.00691197	9.90667515	-0.80011532
	C	3.03699663	9.98822290	-0.65081584
	C	3.26711382	11.36105818	-0.64867988
	C	2.30733209	12.23279509	-0.12762395
	C	1.11666760	11.71698603	0.38871994
	C	0.88184859	10.34328496	0.38889746
	C	2.73685191	4.47901314	-0.08580287
	C	2.30810236	3.29748181	-0.71961971
	C	3.08539185	2.14651524	-0.67276680
	C	4.31546760	2.11305747	0.00673131
	C	4.74047616	3.29395086	0.64170152
	C	3.97389962	4.44988810	0.59216821
	C	5.13549343	0.87889375	0.05265570
	C	6.53993863	0.93944183	0.03646865
	C	7.31148584	-0.21964663	0.07833674
	C	6.70350092	-1.48045551	0.13602344
	C	5.30437982	-1.55058622	0.15272898
	C	4.53420491	-0.39050682	0.11266253
	C	7.53036731	-2.72523675	0.17777235
	C	7.94925915	-3.23447901	1.41957550
	N	8.72315193	-4.39735889	1.47792453
	B	9.19773671	-5.23933687	0.26109182
	N	8.64882771	-4.52914516	-1.00722603
	C	7.87552354	-3.36459691	-1.02604713
	C	-3.59582699	3.80837318	-0.08044114
	C	-4.79558467	3.49448625	-0.75311814
	C	-5.30417831	2.20312904	-0.75291029
	C	-4.64621853	1.16391365	-0.07089772
	C	-3.45372730	1.48028374	0.60250205
	C	-2.93341628	2.76893910	0.59956613
	C	-5.19261790	-0.21411106	-0.06269323
	C	-5.07105361	-1.03627708	1.07129571
	C	-5.58920805	-2.32928264	1.08188460
	C	-6.24321900	-2.84612841	-0.04414694
	C	-6.36557558	-2.03536493	-1.18017049
	C	-5.85095890	-0.74094808	-1.18770296
	C	-6.80052282	-4.23311187	-0.03368872
	C	-8.09665099	-4.45175116	0.46640139
	N	-8.63384930	-5.74221356	0.48712994
	B	-7.92925963	-7.03204702	-0.01741575
	N	-6.52802860	-6.59722186	-0.52923406
	C	-6.02026985	-5.29459692	-0.52479373
	C	-5.59714936	-7.42191396	-1.04805551
	C	-4.43977417	-6.67869632	-1.39479516
	C	-4.69432316	-5.34183710	-1.07104923
	C	-9.08191675	-3.56083894	1.00828468

2a	C	5.53694100	-0.26893800	0.12569000
	N	4.45486200	0.64817500	0.14248000
	B	2.99153200	0.17868100	-0.00532000
	N	2.96879200	-1.35553900	-0.17671200
	C	4.16431800	-2.11972500	-0.18916600
	N	5.37715400	-1.58441200	-0.03834200
	C	1.90603300	-2.24200400	-0.22364200
	C	2.42618700	-3.56998700	-0.29308800
	C	3.82646800	-3.52280000	-0.29108400
	C	6.77949800	0.46537200	0.21430700
	C	6.41170400	1.81845500	0.23858100
	C	4.98995500	1.92366500	0.19493800
	F	2.20244300	0.52006000	1.16278400
	F	2.40965600	0.85381300	-1.14868700
	C	4.75062400	-4.66126800	-0.37668600
	C	8.14122600	-0.08243100	0.26894000
	C	4.29787500	-5.96438100	-0.03983600
	C	5.15180700	-7.07291500	-0.14118900
	C	6.48050300	-6.90512100	-0.58278000
	C	6.94328800	-5.61702300	-0.91781500
	C	6.09116200	-4.50523300	-0.81591000
	C	9.24802800	0.74370400	-0.06168500
	C	10.56053000	0.25333900	0.00921000
	C	10.79879600	-1.07643500	0.41354500
	C	9.70949800	-1.90760200	0.74251800
	C	8.39440600	-1.41988500	0.67119500
	C	4.26282300	3.20153000	0.20195900
	C	2.97082200	3.37074100	0.75996900
	C	2.35022400	4.62998800	0.76598400
	C	3.01439300	5.73203200	0.20447900
	C	4.29359400	5.59782300	-0.36137700
	C	4.90918600	4.33833200	-0.35439200
	Br	2.14081200	7.49484600	0.20704700
	C	0.47242300	-1.92606500	-0.20509400
	C	-0.42112100	-2.89291100	0.33221900
	C	-1.80045800	-2.66838500	0.36212000
	C	-2.35762800	-1.47035200	-0.15137100
	C	-1.46604900	-0.51266100	-0.69300600
	C	-0.08304900	-0.72698600	-0.71902700
	C	-3.82447200	-1.22779400	-0.11959200
	C	-4.34743400	0.08456300	-0.00731300
	C	-5.72869600	0.31720500	0.01521100
	C	-6.64633300	-0.75938600	-0.05385400
	C	-6.12978500	-2.07402700	-0.15718900
	C	-4.74782900	-2.29990300	-0.19881800
	C	-8.10993900	-0.51662100	-0.01800900
	C	-8.69910400	0.43817400	-0.88183000
	N	-10.08837900	0.69340700	-0.85005500
	B	-11.10432800	-0.01669100	0.05926800
	N	-10.33035100	-1.03000000	0.91804500
	C	-8.93350700	-1.23748100	0.88085800
	C	-10.85423900	-1.82114600	1.89363900
	C	-9.81871800	-2.56019300	2.52171500
	C	-8.61526500	-2.19145300	1.89784500
	C	-8.13930400	1.24479700	-1.92202100
	C	-9.18769300	1.98636200	-2.49113600
	C	-10.37489700	1.61760300	-1.80708600
	F	-12.10867000	-0.68498900	-0.73546500
	F	-11.78644100	0.93723700	0.90297800
	H	1.81681300	-4.45317000	-0.40974000
	H	7.07756600	2.66049700	0.35207200
	H	3.28249300	-6.10640400	0.32101700
	H	4.78778600	-8.06165200	0.12642200
	H	7.14224300	-7.76382100	-0.66427700
	H	7.96450500	-5.47982000	-1.26445500
	H	6.45259900	-3.51815900	-1.08003300

C	-10.19074375	-4.34424936	1.34602160
C	-9.87411922	-5.68559059	1.01121998
C	8.83564702	-4.94411555	-2.27563895
C	8.18957240	-4.05300042	-3.17025547
C	7.58191832	-3.05845375	-2.39660253
C	7.74087269	-2.78158070	2.76493732
C	8.39960274	-3.68871398	3.60152939
C	8.99643298	-4.66994215	2.76897355
C	6.97531414	-1.57757802	3.23320254
C	8.50355951	-3.64346674	5.10318489
C	9.72319120	-2.85337257	5.61362270
C	9.82361375	-5.84996289	3.16796689
C	6.78415346	-1.90968255	-2.94332718
C	8.15546767	-4.19810777	-4.66885803
C	6.96508842	-5.03053579	-5.18105135
C	9.61866414	-6.17758864	-2.59393417
C	-8.99025965	-2.07376355	1.19558631
C	-10.71538483	-6.91029312	1.17946205
C	-11.47881673	-3.88629416	1.97757371
C	-11.44811794	-3.89576396	3.51746347
C	-3.73019847	-4.20858274	-1.27346501
C	-3.19585048	-7.24932719	-2.02305148
C	-3.22879970	-7.25364454	-3.56291216
C	-5.84148272	-8.88913769	-1.20115837
F	-8.66019915	-7.60533415	-1.06179468
F	-7.79916860	-7.94494910	1.03285582
F	8.68273300	-6.53662979	0.33927090
F	10.59423076	-5.28012213	0.22757608
H	-5.09247373	6.24508081	-0.18803754
H	3.68994366	7.17785059	-0.08345853
H	-5.63692576	8.36123877	0.71372021
H	-6.55202070	10.64727411	0.59128343
H	-5.20126526	12.48360018	-0.41041949
H	-2.92882170	11.99378833	-1.29875961
H	-2.01886392	9.70024126	-1.19271837
H	3.77886289	9.32136426	-1.08046608
H	4.19383110	11.75180446	-1.06009051
H	2.48666924	13.30446327	-0.12466663
H	0.36697832	12.38669444	0.80146038
H	-0.04119028	9.95093009	0.79765655
H	1.37431649	3.28861742	-1.26462849
H	2.74214197	1.26279648	-1.20256458
H	5.66695440	3.29776251	1.20822722
H	4.31761665	5.33340128	1.12057946
H	7.03513916	1.90335958	-0.03608806
H	8.39544791	-0.14804873	0.05579277
H	4.81730965	-2.52031372	0.20708536
H	3.45197134	-0.47069230	0.15449973
H	-5.32297336	4.26878650	-1.30105366
H	-6.23703033	2.00196533	-1.27124862
H	-2.90851809	0.69786671	1.12220655
H	-2.01237526	2.97368166	1.12757922
H	-4.58956221	-0.65072821	1.96517278
H	-5.49222483	-2.94255035	1.97353061
H	-6.86221107	-2.42420648	-2.06488577
H	-5.93770841	-0.14133193	-2.08908154
H	6.95112909	-1.54184367	4.32569096
H	7.42587528	-0.64271054	2.88196970
H	5.94081003	-1.58005908	2.87550014
H	7.59090846	-3.20546699	5.52470256
H	8.54878014	-4.66535969	5.49952298
H	9.75781220	-2.85177931	6.70937452
H	10.65811304	-3.29021770	5.24496582
H	9.68768780	-1.81259538	5.27260220
H	9.45098004	-6.75869358	2.68601198
H	10.86159524	-5.72126137	2.84016316
H	9.81463959	-5.98892584	4.25120735
H	7.17704682	-0.94121931	-2.61787945
H	6.79409093	-1.92420528	-4.03652789
H	5.73743223	-1.94696792	-2.62191938
H	8.12688257	-3.20660365	-5.13644506
H	9.08882648	-4.65884609	-5.01501605
H	6.98526410	-5.11101125	-6.27420900
H	6.98542227	-6.04424079	-4.76534582
H	6.01238829	-4.57344876	-4.89088860
H	9.74629270	-6.29646863	-3.67194809
H	9.07956600	1.76477800	-0.39367000
H	11.39388300	0.90023100	-0.25304800
H	11.81566900	-1.45663600	0.47124700
H	9.88479600	-2.93223100	1.06082200
H	7.56184200	-2.06353200	0.93032300
H	2.45319000	2.53082000	1.20576600
H	1.36436300	4.74175800	1.20550900
H	4.79896500	6.45003000	-0.80397800
H	5.88715500	4.23610800	-0.81464400
H	-0.02874600	-3.80717800	0.76740000
H	-2.44454900	-3.41378900	0.82013800
H	-1.85605600	0.40349600	-1.12738600
H	0.56000400	0.02352300	-1.16054400
H	-3.67161000	0.92863500	0.09454700
H	-6.09857100	1.33149400	0.13335200
H	-6.81272200	-2.91330900	-0.25113200
H	-4.38653900	-3.31650600	-0.32497700
H	-11.91385600	-1.81920600	2.10676900
H	-9.94887800	-3.25975700	3.33440600
H	-7.62249300	-2.53737200	2.14481100
H	-7.10104800	1.25344700	-2.21903100
H	-9.12385500	2.69602700	-3.30296000
H	-11.38714000	1.96018500	-1.96904300

	H	10.60337246	-6.13907274	-2.11801489				
	H	9.11294347	-7.06603390	-2.19938018				
	H	-9.95226870	-1.67106699	1.52428207				
	H	-8.24381085	-1.79982890	1.94974470				
	H	-8.70780711	-1.55733068	0.27313507				
	H	-10.78126899	-7.46127713	0.23627108				
	H	-10.26369845	-7.59006760	1.91072736				
	H	-11.72233066	-6.65371608	1.51537229				
	H	-11.72250762	-2.87482759	1.63072523				
	H	-12.30391355	-4.52152115	1.63275563				
	H	-12.40631205	-3.55899922	3.93019983				
	H	-11.24795644	-4.90247188	3.90122545				
	H	-10.66198704	-3.23441312	3.89872558				
	H	-3.56904864	-3.63390045	-0.35626473				
	H	-2.76019362	-4.58812091	-1.60610170				
	H	-4.08318067	-3.49896883	-2.03026717				
	H	-2.31815834	-6.68515736	-1.68536225				
	H	-3.04067516	-8.27484831	-1.66611842				
	H	-2.30565895	-7.67981395	-3.97282675				
	H	-4.07164224	-7.84550072	-3.93729944				
	H	-3.33832562	-6.23679368	-3.95632304				
	H	-4.94019510	-9.40589832	-1.53758499				
	H	-6.17108421	-9.32293873	-0.25212910				
	H	-6.64274703	-9.07179538	-1.92610618				
E	-4073.225211				E	-2545.155449		
2b	C	-6.08142500	-0.98140200	0.08328500	**3**	C	-3.39272082	-0.09747388	-0.89104728
	N	-4.69258700	-1.12386600	0.12633800		N	-3.16067151	-1.14493447	0.00714341
	B	-3.72034300	0.10632300	0.03082600		B	-2.55880987	-0.90377824	1.44807108
	N	-4.63095800	1.38382600	-0.04722400		N	-2.40727919	0.65516024	1.59878494
	C	-6.02409600	1.31243900	0.02111600		C	-2.72534727	1.54563315	0.56895927
	N	-6.70714500	0.18202700	0.05789000		N	-3.18368230	1.17747640	-0.61452596
	C	-4.28868200	2.70551800	-0.01789800		C	-1.84904679	1.38659553	2.61028272
	C	-5.46950900	3.48865900	0.03718300		C	-1.82960681	2.75340200	2.23646616
	C	-6.57063000	2.64429000	0.05795700		C	-2.38759500	2.88488050	0.97181416
	C	-6.69603300	-2.28357000	0.05990300		C	-3.99775423	-0.61729553	-2.08949656
	C	-5.63951200	-3.18301200	0.06412300		C	-4.16921187	-1.97224032	-1.84838327
	C	-4.41893700	-2.46167400	0.09499500		C	-3.66158774	-2.28370757	-0.55997829
	F	-2.92289500	0.22128100	1.16680800		F	-3.47103874	-1.41943293	2.36294803
	F	-2.95023900	-0.04736000	-1.11927600		O	-1.28302106	-1.55577191	1.68149303
	C	-7.98347400	3.03305800	0.09432000		C	-2.58123156	4.12188967	0.21131063
	C	-8.12737800	-2.59950100	0.04897900		C	-4.37168929	0.12606224	-3.29516734
	C	-8.37414600	4.28367400	-0.42433600		C	-3.59083949	4.24885449	-0.76289987
	C	-9.70448000	4.69122600	-0.38412200		C	-3.76429961	5.44820517	-1.45063344
	C	-10.67683400	3.85902600	0.17680100		C	-2.94046503	6.54390027	-1.18323529
	C	-10.30463800	2.61647700	0.69439800		C	-1.93461530	6.43171342	-0.21965845
	C	-8.97402700	2.20405000	0.65647200		C	-1.75731320	5.23538261	0.46936293
	C	-8.57265900	-3.82784400	0.57680700		C	-5.38952624	-0.37014549	-4.13367604
	C	-9.92264500	-4.16661600	0.56037900		C	-5.74735087	0.30123510	-5.29918997
	C	-10.86062100	-3.28631300	0.01454100		C	-5.09628771	1.48553090	-5.65478777
	C	-10.43419400	-2.06516600	-0.51203300		C	-4.08659803	1.99072497	-4.83262499
	C	-9.08372300	-1.72152100	-0.49785200		C	-3.72440922	1.32119671	-3.66554145
	C	-3.09757000	-3.09459800	0.07333600		C	-3.72014097	-3.62846565	0.02570544
	C	-1.96163500	-2.56217600	0.71190100		C	-2.77268950	-4.13614648	0.93463688
	C	-0.75152600	-3.24488100	0.68930200		C	-2.88167802	-5.44004044	1.41242303
	C	-0.61371800	-4.48014100	0.03280300		C	-3.93268796	-6.26363244	1.00482324
	C	-1.74930400	-5.00955300	-0.60628000		C	-4.88410271	-5.77156141	0.10799181
	C	-2.96250800	-4.33614700	-0.58326600		C	-4.77720591	-4.47290494	-0.37856831
	C	0.68107800	-5.19990900	0.01401700		C	-1.34275341	0.88953723	3.89522695
	C	0.73194800	-6.60467100	0.05268700		C	-0.25290459	1.56852970	4.48032489
	C	1.94590700	-7.28282700	0.02973900		C	0.25212339	1.17893878	5.71688338
	C	3.16183400	-6.57900100	-0.01884200		C	-0.32703672	0.10867609	6.40327242
	C	3.11697500	-5.17438300	-0.05319100		C	-1.40988065	-0.56775638	5.83774143
	C	1.90009700	-4.50105600	-0.04319700		C	-1.91565514	-0.18835068	4.59626427
	C	4.45343400	-7.30313900	-0.03537800		C	-0.06897242	-1.25555459	1.16226834
	C	4.67797300	-8.31537700	-0.98724300		C	0.13498408	-0.55499855	-0.03671163
	N	5.87562200	-9.02911100	-1.01075100		C	1.43122365	-0.31787580	-0.49719557
	B	7.05834900	-8.87733300	-0.00069400		C	2.54845662	-0.77145467	0.21219935
	N	6.69138000	-7.63528200	0.87615300		C	2.33822443	-1.47662078	1.40659352
	C	5.46290500	-6.97422000	0.88834700		C	1.05107221	-1.71388222	1.87628771
	C	-2.93579900	3.26873700	-0.02009400		C	3.93193412	-0.51006657	-0.28724309
	C	-2.71938900	4.48887400	0.65389500		C	4.59182539	0.67294222	0.08842275
	C	-1.47148200	5.09638200	0.65851000		N	5.88982279	0.93801185	-0.36759787
	C	-0.38317300	4.52192900	-0.02250100		B	6.73682511	0.01835755	-1.29119708
	C	-0.60311700	3.30967600	-0.69924500		N	5.85809237	-1.22712536	-1.59530165
	C	-1.84691400	2.68988100	-0.69862000		C	4.55788026	-1.45040845	-1.12251007
	C	0.94794700	5.17242400	-0.02573000		C	6.22191480	-2.27046386	-2.36799248

	C	1.77909800	5.11959400	-1.15874300		C	5.16213703	-3.19766487	-2.41588833
	C	3.02539100	5.73684700	-1.16737400		C	4.11108819	-2.70907604	-1.64704203
	C	3.49741600	6.41935700	-0.03277900		C	4.18615499	1.77099488	0.91745006
	C	2.67357000	6.46956600	1.10493800		C	5.25760339	2.65846320	0.92814058
	C	1.42145800	5.86411900	1.10331100		C	6.29017819	2.12463510	0.13249194
	C	4.82796600	7.06956100	-0.04094400		C	2.80041588	-3.41350175	-1.45382481
	C	5.15718100	7.98095800	-1.06151200		C	7.55601489	-2.35782746	-3.03532494
	N	6.41005900	8.59157800	-1.10521300		C	2.89635896	1.98819736	1.65324673
	B	7.59958400	8.32575400	-0.12710100		C	7.63246465	2.71416864	-0.15700543
	N	7.01200400	7.40465800	0.99226000		F	7.90967441	-0.36887081	-0.63741369
	C	5.76001800	6.78956400	0.97559300		F	7.05022722	0.68679656	-2.47758270
	C	7.68407500	6.94576000	2.06010000		H	-1.50743828	3.55491235	2.88537216
	C	6.89845100	6.01897100	2.77244700		H	-4.55518991	-2.70482365	-2.54202979
	C	5.69362500	5.90975900	2.08931800		H	-4.23757880	3.40554586	-0.97234356
	C	4.37425500	8.52005500	-2.11763000		H	-4.55222957	5.52815666	-2.19464214
	C	5.16872800	9.43984100	-2.79057900		H	-3.07978324	7.47764035	-1.72112799
	C	6.41365600	9.45654800	-2.13190900		H	-1.28338541	7.27569128	-0.00929369
	C	7.44672800	-7.12280400	1.86063800		H	-0.95786513	5.15088152	1.19972861
	C	6.74019600	-6.11617700	2.54705100		H	-5.91776325	-1.27692684	-3.85398636
	C	5.49036100	-6.02687300	1.94704600		H	-6.53939930	-0.09646422	-5.92778592
	C	3.89163400	-8.75055700	-2.08782000		H	-5.37464530	2.00983127	-6.56485198
	C	4.62058000	-9.72825800	-2.75334500		H	-3.57177021	2.90841637	-5.10379207
	C	5.83869000	-9.86608300	-2.05978300		H	-2.93709879	1.71762766	-3.03602633
	F	8.04637800	9.52046600	0.41359000		H	-1.95079941	-3.51247662	1.25979769
	F	8.62501900	7.66466800	-0.78790300		H	-2.13582401	-5.81453130	2.10808918
	F	8.24228800	-8.65556600	-0.68484800		H	-4.01243952	-7.27858874	1.38437465
	F	7.15196400	-10.00559600	0.80187000		H	-5.71373790	-6.39740183	-0.20869039
	H	-5.48477100	4.56881600	0.05032900		H	-5.53716902	-4.09480517	-1.05464737
	H	-5.71089300	-4.26088600	0.05509400		H	0.21574445	2.38862374	3.94532030
	H	-7.63039600	4.92749900	-0.88471500		H	1.10015006	1.70795367	6.14264606
	H	-9.98404300	5.65674600	-0.79680900		H	0.06333785	-0.19506057	7.37071331
	H	-11.71529500	4.17703100	0.20953900		H	-1.87004147	-1.39699434	6.36789750
	H	-11.05295500	1.96519500	1.13790700		H	-2.75737865	-0.71762707	4.17167133
	H	-8.69263100	1.24194100	1.06658400		H	-0.70685793	-0.20268131	-0.62013899
	H	-7.85512400	-4.50861200	1.02555300		H	1.57212331	0.22683192	-1.42716327
	H	-10.24417200	-5.11599400	0.97989200		H	3.19193314	-1.83723503	1.97441002
	H	-11.91444400	-3.55063200	0.00034400		H	0.88612481	-2.24933044	2.80607944
	H	-11.15565400	-1.37689200	-0.94403100		H	5.17546951	-4.13137780	-2.96386404
	H	-8.76052800	-0.77563300	-0.91481900		H	5.30265830	3.60292963	1.45574450
	H	-2.03384800	-1.62209300	1.24107400		H	1.95374842	-2.81174215	-1.80062945
	H	0.09626400	-2.82293500	1.22092400		H	2.80115397	-4.35374288	-2.01418381
	H	-1.67281500	-5.94300100	-1.15583600		H	2.60734252	-3.64557928	-0.40117763
	H	-3.80943700	-4.75737100	-1.11526900		H	7.63739176	-3.28601135	-3.60646214
	H	-0.18943200	-7.17364800	0.13268900		H	7.70745589	-1.50774196	-3.70907536
	H	1.95806200	-8.36667800	0.08630400		H	8.36173651	-2.32055642	-2.29444557
	H	4.04198500	-4.61134200	-0.12614100		H	2.03657603	2.03358727	0.97638161
	H	1.89496100	-3.41755000	-0.11238800		H	2.68690259	1.18581318	2.36847239
	H	-3.53472800	4.95323800	1.19930000		H	2.94413545	2.93273955	2.20512583
	H	-1.34505700	6.04128400	1.17856300		H	7.76546716	2.86202763	-1.23409296
	H	0.22061800	2.82784400	-1.21766100		H	7.74617383	3.67418418	0.35269809
	H	-1.97813900	1.75511500	-1.22599300		H	8.43001419	2.03798888	0.16874567
	H	1.43643300	4.60820500	-2.05317000					
	H	3.65019600	5.67580600	-2.05282700					
	H	3.01121900	7.00430200	1.98702400					
	H	0.81135900	5.90971100	2.00038300					
	H	8.69101500	7.28575800	2.26268400					
	H	7.19477300	5.49733400	3.67196200					
	H	4.85546500	5.27467600	2.33746600					
	H	3.34515500	8.26555200	-2.32691600					
	H	4.89676900	10.04421700	-3.64486600					
	H	7.29204400	10.05064700	-2.34628600					
	H	8.44494700	-7.49974600	2.03970400					
	H	7.11222200	-5.53884200	3.38209500					
	H	4.67642300	-5.37261900	2.22418300					
	H	2.91936300	-8.36206000	-2.35483200					
	H	4.33209900	-10.27519500	-3.64029800					
	H	6.67741500	-10.51496400	-2.27417000					
E	-3444.148683				E	-2666.133471			
4a	C	-2.99110800	0.08415800	-0.82301600	**4b**	C	-1.60467500	-2.63590800	-1.48711300
	N	-2.66752400	-1.21079700	-0.40143100		N	-0.57460700	-1.69228600	-1.40683200
	B	-2.01885200	-1.49907800	1.00659100		B	0.04009300	-1.19146000	-0.03503100
	N	-1.93954400	-0.11385600	1.74335900		N	-0.72758600	-2.01632300	1.08245200
	C	-2.34601000	1.08185000	1.14293200		C	-1.75299300	-2.92594800	0.78526600
	N	-2.83506800	1.16681700	-0.08186600		N	-2.17039100	-3.20257500	-0.43492300
	C	-1.37561200	0.20710500	2.94756600		C	-0.49437000	-2.10323900	2.42585600
	C	-1.43978600	1.61059600	3.12858000		C	-1.40305300	-3.02816100	2.99927600

C	-2.05810500	2.18210200	2.02405000
C	-3.62143300	0.02454500	-2.11567100
C	-3.71484600	-1.32762000	-2.40980400
C	-3.13642300	-2.07575800	-1.35185400
F	-2.85255100	-2.38889000	1.67298200
C	-2.34544300	3.60143200	1.80323000
C	-4.08447800	1.14694800	-2.93513100
C	-3.39890200	4.02902400	0.97135500
C	-3.66084400	5.38701200	0.80221200
C	-2.88371700	6.34542500	1.45666400
C	-1.83535200	5.93530900	2.28466300
C	-1.56958100	4.57983500	2.45610400
C	-5.11595300	0.94701400	-3.87394200
C	-5.55754500	1.98893900	-4.68423100
C	-4.97843100	3.25608700	-4.57564400
C	-3.95606300	3.46986900	-3.64843000
C	-3.51032400	2.42948000	-2.83585700
C	-3.10324200	-3.54295400	-1.32717400
C	-2.09632600	-4.30083900	-0.70006400
C	-2.12125600	-5.69229600	-0.75754600
C	-3.14561500	-6.36000700	-1.43125300
C	-4.15512100	-5.62159500	-2.05352100
C	-4.13223400	-4.23173700	-2.00603400
C	-0.79097300	-0.71257100	3.93075400
C	0.29831900	-0.24909000	4.69837000
C	0.87348200	-1.05026000	5.67970400
C	0.36618000	-2.32870000	5.92490900
C	-0.71542500	-2.79690800	5.17587500
C	-1.29085300	-2.00363300	4.18578700
O	-0.69480300	-2.10558900	0.94343400
C	0.46950100	-1.56493500	0.53254200
C	0.58058000	-0.42961900	-0.28872000
C	1.83455600	0.03971800	-0.66802400
C	3.01548100	-0.60871400	-0.26547900
C	2.89134800	-1.75455600	0.54639900
C	1.64640200	-2.21671600	0.94503900
C	4.33989700	-0.10944200	-0.67990000
C	5.29033900	-0.99296600	-1.23240500
N	6.55915900	-0.54988100	-1.60444000
B	7.09796100	0.91135300	-1.49540400
N	5.90305600	1.75116700	-0.94160500
C	4.66564200	1.25529500	-0.53186900
C	5.94169300	3.06274700	-0.65154200
C	4.73771000	3.46468400	-0.04540000
C	3.93788900	2.33033700	0.04247500
C	5.19069400	-2.36457800	-1.58546200
C	6.40569900	-2.73512600	-2.15102100
C	7.21792600	-1.58641100	-2.14939700
F	8.16499700	0.96928600	-0.60897600
F	7.47534600	1.37130400	-2.74882400
H	-1.12863100	2.11987900	4.02926600
H	-4.09410800	-1.76168900	-3.32326000
H	-4.00998300	3.29197900	0.46478600
H	-4.48136400	5.69693500	0.16078700
H	-3.09231200	7.40334000	1.32299700
H	-1.22042000	6.67290200	2.79303500
H	-0.73841400	4.27192200	3.08382200
H	-5.58856900	-0.02789400	-3.94965000
H	-6.35859000	1.81390200	-5.39717600
H	-5.32201000	4.06967100	-5.20855300
H	-3.49674900	4.45071400	-3.56091500
H	-2.71367400	2.60276700	-2.12263900
H	-1.29298000	-3.80111600	-0.17590600
H	-1.33047300	-6.25799400	-0.27269600
H	-3.15972600	-7.44575700	-1.46906200
H	-4.96463300	-6.12824300	-2.57138000
H	-4.93611100	-3.67102900	-2.47175300
H	0.71186100	0.73481900	4.50017400
H	1.72049100	-0.67850200	6.24937700
H	0.81119100	-2.95456300	6.69356500
H	-1.11984400	-3.78741300	5.36497300
H	-2.13089200	-2.37598700	3.61604400
H	-0.30468800	0.07812500	-0.65049700
H	1.89817000	0.90322400	-1.32267500
H	3.78595800	-2.25964600	0.89680200
H	1.55475600	-3.08090000	1.59528000

C	-2.20620700	-3.55505500	1.99981000
C	-1.84503300	-2.97018200	-2.86533500
C	-0.90231100	-2.24103700	-3.58427800
C	-0.15311900	-1.45501100	-2.68230800
O	1.42356200	-1.59222500	0.03114100
C	-3.28451500	-4.53541600	2.15888600
C	-2.85237200	-3.88911100	-3.39794800
C	-3.65975700	-5.41535000	1.12469800
C	-4.67279200	-6.35083300	1.32515600
C	-5.33231300	-6.43008600	2.55372000
C	-4.97108900	-5.56221800	3.58754500
C	-3.95863300	-4.62708500	3.39307700
C	-2.63465600	-4.51947400	-4.63932000
C	-3.58553700	-5.37954900	-5.18069600
C	-4.77772600	-5.62869400	-4.49539100
C	-5.00808300	-5.01037300	-3.26429600
C	-4.05908500	-4.14859500	-2.71850000
C	0.89317000	-0.50844800	-3.10958300
C	0.83260100	0.86342800	-2.81404600
C	1.78402400	1.73748000	-3.33770300
C	2.81236500	1.25772700	-4.15185300
C	2.88105000	-0.10508900	-4.45097600
C	1.92180200	-0.97965600	-3.94516700
C	0.54605000	-1.42468100	3.21181900
C	1.15312400	-2.15623500	4.25489000
C	2.11185900	-1.57001800	5.07519400
C	2.47565000	-0.23476900	4.88405100
C	1.87620700	0.50247900	3.86181800
C	0.92388400	-0.08270900	3.02981800
O	-0.13830200	0.24522800	0.12971000
C	-1.27742200	0.97426000	0.16018100
C	-2.57558100	0.45730300	0.01405800
C	-3.67746800	1.30583800	0.07767900
C	-3.53236500	2.69026100	0.26953500
C	-2.22668900	3.20046800	0.40148000
C	-1.12362400	2.35970400	0.35609000
C	-4.70743100	3.58296800	0.32915800
C	-5.79180700	3.27719100	1.17587700
N	-6.91923700	4.09693500	1.22788600
B	-7.08939800	5.47677800	0.51364000
N	-5.83890900	5.61717700	-0.41142700
C	-4.75414700	4.74314800	-0.46988300
C	-5.64305100	6.58391400	-1.32312400
C	-4.42904200	6.37501800	-2.00391200
C	-3.87192800	5.21528500	-1.47767100
C	-5.98448100	2.21703100	2.10105400
C	-7.23288400	2.40002400	2.68442000
C	-7.77211400	3.57272700	2.12348000
F	-8.24718400	5.48948300	-0.24898000
F	-7.10806500	6.49458100	1.45739800
C	2.62858600	-0.99378800	0.04991800
C	2.85527200	0.39342000	0.03515700
C	4.15580200	0.88516800	0.04959600
C	5.27183600	0.03007600	0.10359800
C	5.03115700	-1.35835900	0.13031600
C	3.73893800	-1.85863200	0.09379600
C	6.64090900	0.57300800	0.12667500
C	7.02904700	1.55237200	-0.81308600
N	8.30642400	2.10992100	-0.79124500
B	9.43211300	1.79367400	0.24192700
N	8.88596400	0.60302200	1.09275000
C	7.57991100	0.11340100	1.07460600
C	9.54150100	0.00058800	2.09951900
C	8.68988300	-0.89631900	2.76918700
C	7.45317100	-0.81909300	2.13709600
C	6.34695300	2.07751300	-1.94164500
C	7.21759400	2.95712500	-2.57735100
C	8.41523900	2.94300300	-1.84007000
F	9.65741200	2.89198200	1.06251200
F	10.59495700	1.42753500	-0.41948600
H	-1.43645700	-3.26877100	4.05198000
H	-0.79248200	-2.19380300	-4.65853500
H	-3.14939000	-5.36476300	0.17094900
H	-4.94311600	-7.02583900	0.51767200
H	-6.12152300	-7.16134500	2.70515000
H	-5.48269900	-5.61008100	4.54487100

	H	6.82376400	3.64815500	-0.87444200
	H	4.50080600	4.46465900	0.29108100
	H	2.95146400	2.25755100	0.47683700
	H	4.31498100	-2.98312000	-1.45260600
	H	6.68328000	-3.70666500	-2.53612200
	H	8.22561900	-1.46101500	-2.52257800
E	-2508.856340			
8	C	-0.68950400	1.14235700	0.11085900
	N	0.70322100	1.25165500	0.11951600
	B	1.64662500	0.00047000	0.00022900
	N	0.70406500	-1.25121800	-0.11946100
	C	-0.68871500	-1.14281100	-0.11078000
	N	-1.34357900	-0.00042500	0.00000700
	C	1.00975400	-2.58110500	-0.09925400
	C	-0.19252100	-3.33332100	-0.10745600
	C	-1.27076700	-2.45951900	-0.13484700
	C	-1.27239800	2.45877100	0.13483400
	C	-0.19468200	3.33319200	0.10734100
	C	1.00808400	2.58171500	0.09923100
	F	2.42964700	0.16138100	-1.13950800
	F	2.42923400	-0.15987400	1.14032500
	C	2.34820500	-3.18135700	-0.07348800
	C	-2.69386500	-2.80614700	-0.16849300
	C	-2.69568800	2.80460400	0.16846800
	C	2.34616800	3.18271400	0.07337000
	C	-3.66101300	-1.93709000	-0.71052900
	C	-5.00367900	-2.30780300	-0.74965700
	C	-5.41131100	-3.54830200	-0.25391700
	C	-4.46251700	-4.42012000	0.28676500
	C	-3.12042400	-4.05334600	0.32915600
	C	2.50711400	-4.41478800	0.59254500
	C	3.74078800	-5.05729200	0.62224400
	C	4.84187100	-4.48815100	-0.02249400
	C	4.69597900	-3.27047600	-0.69008700
	C	3.46568700	-2.61779600	-0.71755500
	C	3.46395700	2.61976600	0.71746800
	C	4.69391600	3.27306200	0.68993300
	C	4.83917800	4.49076600	0.02225100
	C	3.73778700	5.05932200	-0.62247800
	C	2.50443700	4.41620600	-0.59270200
	C	-3.12276600	4.05211100	-0.32799900
	C	-4.46504800	4.41816000	-0.28562300
	C	-5.41356700	3.54529200	0.25385600
	C	-5.00543900	2.30448800	0.74841100
	C	-3.66257300	1.93450000	0.70931100
	H	-0.23361500	-4.41129700	-0.16733700

	H	-3.70147900	-3.94162000	4.19532700
	H	-1.70191200	-4.34942900	-5.16907100
	H	-3.39438200	-5.86026900	-6.13611800
	H	-5.52109800	-6.29856100	-4.91860000
	H	-5.93570000	-5.19265500	-2.72859500
	H	-4.24943700	-3.66642300	-1.76725400
	H	0.02479800	1.24828200	-2.20385700
	H	1.71564500	2.79889600	-3.11566600
	H	3.55023400	1.94303100	-4.56006900
	H	3.67825200	-0.48666300	-5.08246400
	H	1.97313800	-2.03862900	-4.18081100
	H	0.89023400	-3.19942600	4.39933300
	H	2.57731300	-2.15698200	5.86191000
	H	3.22079500	0.22637300	5.52610500
	H	2.14955300	1.54264400	3.70942900
	H	0.46295600	0.50290300	2.24706600
	H	-2.73782800	-0.59822400	-0.15469500
	H	-4.67011000	0.88820600	-0.05783300
	H	-2.08201200	4.26212600	0.57490900
	H	-0.12183700	2.75920400	0.48144100
	H	-6.37550200	7.36881700	-1.45680000
	H	-4.03029300	6.99778400	-2.79278600
	H	-2.95409500	4.73343300	-1.78211700
	H	-5.27457200	1.42972800	2.30923100
	H	-7.70772000	1.77876900	3.43122900
	H	-8.71519500	4.05960800	2.33349000
	H	2.01625400	1.07301400	0.01132900
	H	4.31206200	1.95963200	0.05448800
	H	5.87028600	-2.04686400	0.13907400
	H	3.55675200	-2.92871000	0.09155600
	H	10.57516400	0.24516100	2.30503300
	H	8.95857000	-1.51280800	3.61600700
	H	6.55029000	-1.35138800	2.39883400
	H	5.34730200	1.80625600	-2.25006900
	H	7.03392900	3.53315100	-3.47401700
	H	9.33812700	3.47709700	-2.02277600
E	-3396.046071			

	H	-0.23638200	4.41113200	0.16739000
	H	-3.35234800	-0.97518200	-1.10153600
	H	-5.73394500	-1.62555200	-1.17645700
	H	-6.45920400	-3.83379100	-0.28762100
	H	-4.76963000	-5.38461700	0.68201900
	H	-2.39406200	-4.72795500	0.77295300
	H	1.66238600	-4.85347600	1.11456000
	H	3.84379000	-5.99976300	1.15284700
	H	5.80561000	-4.98961400	-0.00302700
	H	5.54597400	-2.82367100	-1.19839100
	H	3.36411600	-1.67791000	-1.24274300
	H	3.36285600	1.67991500	1.24281100
	H	5.54414200	2.82673200	1.19826500
	H	5.80266400	4.99271500	0.00271700
	H	3.84030700	6.00181600	-1.15313300
	H	1.65947600	4.85445800	-1.11469900
	H	-2.39665200	4.72757200	-0.77089600
	H	-4.77252800	5.38291600	-0.67995700
	H	-6.46161700	3.83021000	0.28753800
	H	-5.73548100	1.62140400	1.17426300
	H	-3.35355700	0.97234400	1.09940700
E	-1621.658199			

6. References

[1] P.-A. Bouit, K. Kamada, P. Feneyrou, G. Berginc, L. Toupet, O. Maury, C Andraud, *Adv. Mater.* **2009**, *21*, 1151–1154.

[2] M. Koepf, M. Trabolsi, J. A., Wytko, D. Paul, A. M. Albrecht-Gary, J. Weiss, *J. Org. Lett.* **2005**, *7*, 1279–1282.

[3] Z. Liu, S. G. Thacker, S. Fernandez-Castillejo, E. B. Neufeld, A. T. Remaley, R. Bittman, *ChemBioChem* **2014**, *15*, 2087–2096.

[4] a) G. Sathyamoorthi, M.-L. Soong, T. W. Ross, J. H. Boyer, *Heteroat. Chem*. **1993**, *4*, 603–608. b) A. Gorman, J. Killoran, C. O´Shea, T. Kenna, W. M. Gallagher, D. F. O´Shea, *J. Am. Chem. Soc*. **2004**, *126*, 10619–10631.

[5] A. Coskun, E. Deniz, E. U. Akkaya, *Org. Lett*. **2005**, *7*, 5187–5189.

[6] D. Prasannan, D. Raghav, S. Sujatha, H. Kumar, K. Rathinasamy, C. Arunkumar, *RSC Adv*. **2016**, *6*, 80808–80824.